Applied Radiation and Isotopes 233 (2026) 112609

Contents lists available at ScienceDirect

Applied Radiation and Isotopes

journal homepage: www.elsevier.com/locate/apradiso

Thermoluminescence kinetics, time-dependent TL evolution and dosimetric performance of Tb^{3+}-doped $NaCa_4(BO_3)_3$: Effects of preheating and multi-trap structure

Kenan Bulcar [a], E. Aymila Cin [b], Abeer S. Altowyan [c,*], M.B. Coban [d,e], U.H. Kaynar [f], H. Orucu [g], Jabir Hakami [h], Mustafa Topaksu [i], M. Ayvacikli [j], N. Can [h,*]

[a] Igdir University, Vocational School of Health Services, Karaagac Campus, Igdir, 76000, Türkiye
[b] Bakircay University, Graduate School of Natural and Applied Sciences, Menemen, Izmir, Türkiye
[c] Department of Physics, College of Science, Princess Nourah Bint Abdulrahman University, P.O. Box 84428, Riyadh, 11671, Saudi Arabia
[d] Balikesir University, Faculty of Arts and Sciences, Department of Physics, Balikesir, Türkiye
[e] Balikesir University, Science and Technology Application and Research Center, Balikesir, Türkiye
[f] Bakircay University, Faculty of Engineering and Architecture, Department of Fundamental Sciences, Menemen, Izmir, Turkiye
[g] Ege University, Science Faculty, Department of Physics, Izmir, 35040, Türkiye
[h] Jazan University, College of Science, Department of Physical Sciences, Physics Division, P.O. Box 114, Jazan, 45142, Kingdom of Saudi Arabia
[i] Physics Department, Cukurova University, Arts-Sciences Faculty, Adana, 01330, Türkiye
[j] Manisa Celal Bayar University, Hasan Ferdi Turgutlu Technology Faculty, Mechatronics Engineering, Turgutlu, Manisa, Türkiye

ARTICLE INFO

Keywords:
Thermoluminescence
Tb^{3+}-doped borate phosphor
Multi-trap kinetics
Preheating (thermal cleaning)
Time-dependent TL behavior

ABSTRACT

Terbium-doped $NaCa_4(BO_3)_3$ phosphors were synthesized by a microwave-assisted sol–gel combustion route and their thermoluminescence (TL) properties were investigated under β irradiation. The as-irradiated glow curve recorded at IRSL-TL 410 nm displays multiple peaks near 77, 188 and 264 °C, indicating the presence of trapping centers with different thermal stabilities. T_M–T_{stop} measurements combined with Initial Rise (IR) analysis reveal a step-like evolution of activation energies from ~1.0 to ~1.7 eV, indicating a multi-trap system with a quasi-continuous distribution of trapping levels. Computerized glow-curve deconvolution (CGCD) further indicates that a relatively large number of overlapping components between ~1.0 and ~1.8 eV contribute before thermal treatment. After preheating, the glow curve can be reproduced using fewer and deeper components in the ~1.5–1.8 eV range. A controlled preheating step at 225 °C for 7 s acts as a thermal cleaning stage. This step suppresses shallow and intermediate traps near 80–190 °C while largely preserving the high-temperature peak around 260–270 °C. Under these optimized conditions, the isolated dosimetric peak exhibits a linear dose response from ~1.4 to at least 350 Gy. The response remains close to linear with a slight sublinear behavior ($b \approx 0.978$), up to 500 Gy based on both peak height and integrated area. Heating-rate-dependent analysis indicates that instrumental temperature lag contributes to the apparent shift of the peak maximum; therefore, quantitative kinetic parameters were derived from the internally consistent uncorrected VHR analysis. Time-resolved storage experiments show a pronounced, non-monotonic TL evolution. The 270 °C peak intensity first increases by more than an order of magnitude with storage time at room temperature, followed by delayed fading at longer times. The peak temperature and shape remain essentially unchanged. This behavior is consistent with charge redistribution among shallow, metastable and deeper traps in a competitive multi-trap network. Overall, the results indicate that, when a standardized preheating protocol and controlled storage conditions are applied, Tb^{3+}-doped $NaCa_4(BO_3)_3$ provides a stable high-temperature TL peak with wide linearity and promising characteristics for medium-to high-dose radiation dosimetry.

* Corresponding author.
E-mail addresses: asaltowyan@pnu.edu.sa (A.S. Altowyan), ncan@jazanu.edu.sa (N. Can).

https://doi.org/10.1016/j.apradiso.2026.112609
Received 26 February 2026; Received in revised form 1 April 2026; Accepted 1 April 2026
Available online 1 April 2026

1. Introduction

TL is a luminescence phenomenon in which insulating or semiconducting materials emit light upon heating after exposure to ionizing radiation (Pathan et al., 2022; Yukihara et al., 2022; McKeever, 1985; Chen and McKeever, 2011). During irradiation, part of the absorbed energy is stored in defect-related trapping centers, and subsequent thermal stimulation releases the trapped charge carriers, leading to radiative recombination. Within an appropriate dose range, the TL signal intensity is directly related to the absorbed radiation dose, enabling quantitative dose assessment (Satkar et al., 2021). Owing to this property, TL has become a widely used technique in radiation dosimetry, with applications in personal and environmental monitoring, medical and clinical dosimetry, space dosimetry, high-dose industrial processing, and retrospective/archaeological dating. In addition, the TL glow curve, representing light intensity as a function of temperature, provides valuable information on trapping parameters and the defect structure of the material.

Several commercial or well-established TL materials, such as LiF:Mg, Ti (TLD-100), LiF:Mg,Cu,P, $CaSO_4$:Dy, $Li_2B_4O_7$-based phosphors and various natural minerals (e.g. calcite, feldspars), have been successfully employed over dose ranges from sub-mGy up to hundreds of Gy or even kGy levels, often showing linear or quasi-linear dose-response behaviors (Jena et al., 2023; Salas-Juárez et al., 2023; Saran et al., 2025; Liuzzi et al., 2020; Del Sol Fernández et al., 2016; Bilski, 2002). Nevertheless, many commercial TL and optically stimulated luminescence (OSL) dosimeters still suffer from limitations such as signal fading, restricted linear dose-response ranges, energy dependence, complex glow-curve structures, or limited reusability. These drawbacks motivate the search for novel phosphors with improved sensitivity, stability, tissue equivalence, and simpler glow-curve structures.

In this context, rare-earth-doped inorganic hosts have attracted considerable attention, and borate- and borate-related compounds, in particular, have shown promising TL characteristics such as high sensitivity, wide or linear dose-response behavior, low fading, and good reusability (Anishia et al., 2010, 2011; Jakathamani et al., 2021; Khan et al., 2016; Altowyan et al., 2024). Rare-earth-doped borate systems such as $LiMgBO_3$:RE, $LiSrBO_3$:RE, BaB_2O_4:Tb, $NaMgBO_3$:RE, and lanthanum borates have been reported with favorable TL glow curves, extended linear or quasi-linear dose-response ranges, low fading, and good reusability for dosimetric applications (Oza et al., 2022; Jakathamani et al., 2018; Joseph et al., 2023; Liu et al., 2005; Oglakci et al., 2023, 2025) Recent reviews further emphasize the growing interest in borate and phosphate based TL materials for in vivo and clinical dosimetry, highlighting their chemical stability and generally favorable dosimetric performance, including improved energy response for many low-Z hosts (McKeever, 1985; Oglakci et al., 2023). It should be noted that $NaCa_4(BO_3)_3$ is a relatively low-to intermediate-Z oxide host, but not strictly tissue-equivalent in terms of effective atomic number.Among rare earth activators, terbium (Tb^{3+}) has been identified as an efficient dopant in various borate hosts, often providing enhanced TL sensitivity and suitable glow curve structures for dosimetry (Anishia et al., 2011; Liu et al., 2005; Kiran et al., 2025; Reddy et al., 2025). In parallel, $NaCa_4(BO_3)_3$-type borate frameworks have recently been reported as chemically stable, low-Z, and structurally flexible hosts for luminescent applications. Building on these advances, borate-based hosts of the $NaCa_4(BO_3)_3$ family provide a low-Z, structurally flexible platform for Tb^{3+} incorporation, making them attractive candidates for next-generation TL dosimetric materials. These considerations provide the motivation for investigating the TL characteristics and dosimetric potential of Tb-doped $NaCa_4(BO_3)_3$ phosphors.

In this work, Tb^{3+} doped $NaCa_4(BO_3)_3$ phosphors were synthesized, and their TL properties were systematically investigated. To the best of our knowledge, this is the first systematic TL and kinetic investigation of Tb^{3+}-doped $NaCa_4(BO_3)_3$ phosphors, demonstrating that, under optimized readout conditions, the material exhibits a simplified single-peak glow curve, a wide linear dose–response range in the clinically relevant regime, and low fading suitable for dosimetric applications. The TL behavior was further evaluated through dose–response measurements, heating rate dependence, and detailed kinetic analyses, including the variable heating rate (VHR) and initial rise methods, T_M–T_{STOP} experiments, and glow curve deconvolution, providing insight into the trapping and recombination mechanisms of the material.

2. Experiments

2.1. Material preparation and synthesis

Tb^{3+}-doped $NaCa_4(BO_3)_3$ phosphors were synthesized using a microwave-assisted sol–gel combustion technique. This approach was adopted due to its ability to yield highly crystalline rare-earth-doped borate phosphors at relatively lower synthesis times and temperatures compared to conventional solid-state routes (Kiran et al., 2025; Xiang et al., 2024). Sodium nitrate ($NaNO_3$), calcium nitrate ($Ca(NO_3)_2$), and boric acid (H_3BO_3) of analytical grade were used as starting materials. Terbium(III) nitrate ($Tb(NO_3)_3$, 99.9%, Sigma-Aldrich) served as the dopant source, and the Tb^{3+} concentration was varied between 0.5 and 7 wt% with respect to calcium. Urea and glycine were employed as fuel agents to facilitate the combustion process.

The precursors were dissolved sequentially in deionized water under continuous stirring to form a homogeneous solution. The solution was heated at approximately 80 °C until a viscous gel was obtained. Microwave irradiation of the gel initiated a rapid combustion reaction, yielding a fine precursor powder. The as-prepared powders were subsequently calcined at 900 °C in air to improve crystallinity and remove residual organic species. After cooling to room temperature, the final Tb^{3+}-doped $NaCa_4(BO_3)_3$ phosphors were collected and stored in a desiccator prior to characterization.

2.2. Characterization techniques

The phase composition and crystallographic structure of the synthesized samples were examined by X-ray diffraction (XRD) analysis. Measurements were carried out using a Malvern PANalytical Empyrean diffractometer operating with Cu Kα radiation (λ = 1.5406 Å). The diffraction patterns were recorded over an appropriate 2θ range of 10°–80°with a fixed step size of 0.02°, ensuring sufficient angular resolution for phase identification and structural assessment.

TL measurements were performed using a Lexsyg Smart TL/OSL reader (Freiberg Instruments, Germany) located at Bakırçay University. The system is equipped with an internal $^{90}Sr/^{90}Y$ beta radiation source, calibrated to deliver a nominal dose rate of approximately 1.436 Gy/s. The irradiation doses used for kinetic analyses were selected from the calibrated dose range reported in this study. Prior to TL measurements, about 20 mg of Tb^{3+} doped $NaCa_4(BO_3)_3$ powders were gently ground to achieve homogeneity and then pressed into circular pellets with a diameter of 6 mm using a manual hydraulic press. Pelletization was employed to ensure uniform sample geometry and to improve thermal contact between the sample and the heating planchette. Following irradiation, TL glow curves were recorded by heating the samples from room temperature up to 450 °C under a linear heating regime. An initial heating rate of 2 °C/s was selected for standard glow curve acquisition. To evaluate the effect of heating rate on trap kinetics, peak positions, and glow curve shape, additional measurements were conducted using heating rates ranging from 0.1 °C/s to 10 °C/s. All TL measurements were carried out under a continuous flow of nitrogen gas in order to minimize surface oxidation and suppress any parasitic signals arising from chemiluminescence. Background correction was systematically applied to all glow curves using reference measurements obtained from non-irradiated samples under identical experimental conditions. To prevent premature thermal or optical stimulation of charge traps prior to measurement, irradiated samples were stored in opaque containers and

handled under red-light conditions. Furthermore, light homogenization of the powder in an agate mortar before pellet pressing was performed to enhance reproducibility and reduce signal fluctuations associated with non-uniform particle packing.

3. Results and discussions

3.1. X-ray diffraction analysis

The crystal structure and phase composition of the synthesized samples were examined by X-ray diffraction (XRD) analysis prior to TL measurements. The recorded diffraction patterns confirm that the samples are crystalline and do not exhibit any unexpected impurity phases beyond those associated with the host material system. Fig. 1 shows the XRD patterns of the synthesized samples together with the indexed reflections corresponding to the identified crystalline phases. The diffraction peaks were indexed using standard JCPDS reference files (JCPDS#98-017-1421 and JCPDS#98-002-3664). The analysis indicates that the samples predominantly crystallize in the $NaCa_4(BO_3)_3$ host phase, accompanied by a secondary $Ca_3B_2O_6$ (takedaite) phase. The

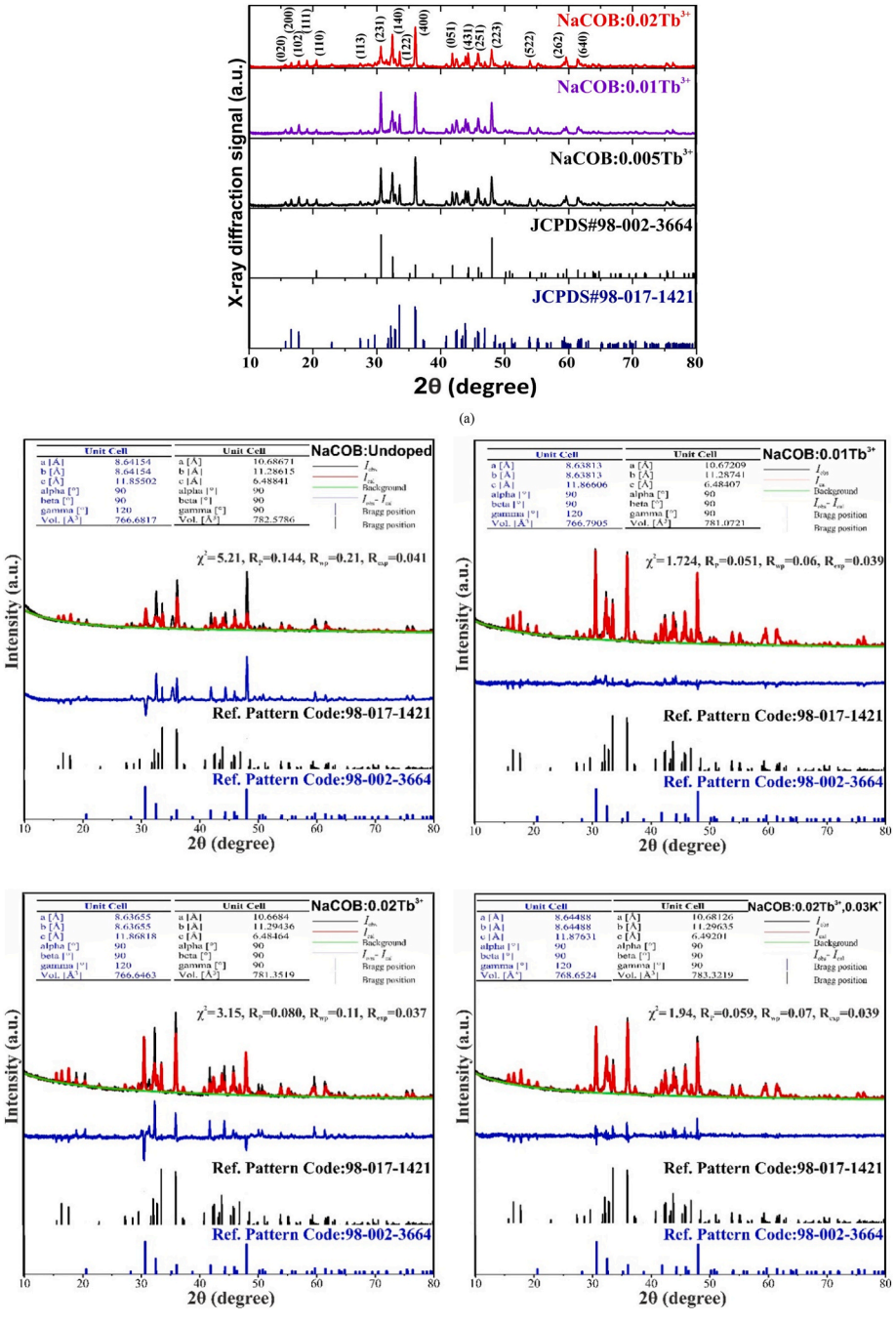

Fig. 1. (a) XRD patterns of Tb-doped $NaCa_4(BO_3)_3$ phosphors with different Tb^{3+} concentrations, along with reference patterns (JCPDS#98-002-3664 and JCPDS#98-017-1421). All diffraction peaks are well indexed to the $NaCa_4(BO_3)_3$ phase, with no significant impurity peaks detected, indicating successful phase formation and high crystallinity. (b) Rietveld refinement of the XRD patterns for undoped and Tb^{3+}-doped $NaCa_4(BO_3)_3$ samples. The refinement confirms that the samples are predominantly composed of the $NaCa_4(BO_3)_3$ phase with a secondary $Ca_3B_2O_6$ (takedaita) phase.

relative phase fractions were estimated to be approximately 63.7% for $NaCa_4(BO_3)_3$ and 36.3% for $Ca_3B_2O_6$. The coexistence of these phases has been previously reported in rare-earth-doped $NaCa_4(BO_3)_3$-based phosphor systems and is considered characteristic of this material family (Shi et al., 2018a).

No noticeable peak shifts, peak splitting, or significant line broadening were observed upon doping, suggesting that the incorporation of dopant ions does not induce substantial distortion of the host lattice, in agreement with reports on structurally stable rare-earth-doped borate and oxyborate phosphors (Singh and Singh, 2021; Kumar et al., 2023). Similar structural stability upon rare-earth doping has been reported in earlier studies on $NaCa_4(BO_3)_3$ phosphors, indicating that the host lattice can accommodate dopant ions without altering its overall phase constitution (Shi et al., 2018a, 2018b).

The preservation of the crystalline structure and the dominance of the $NaCa_4(BO_3)_3$ phase provide a reliable structural basis for the interpretation of the TL behavior discussed in subsequent sections. In particular, the confirmed phase stability ensures that the observed TL response can be primarily attributed to trap-related processes rather than to crystallographic phase transformations (Li et al., 2022; Kaynar et al., 2025). From a crystal-chemical perspective, the incorporation of Tb^{3+} ions into the $NaCa_4(BO_3)_3$ host lattice is expected to occur preferentially at Ca^{2+} sites due to the closer ionic radius match ($Ca^{2+} \approx 1.00$ Å, $Tb^{3+} \approx 0.923$ Å in VIII coordination) compared to Na^+ (≈1.18 Å). Substitution of Tb^{3+} for Ca^{2+} introduces a charge imbalance that can be compensated by the formation of intrinsic defects such as cation vacancies or interstitials, which may act as trapping centers.

Although a partial substitution at Na^+ sites cannot be completely excluded, the combined structural and luminescence results suggest that Tb^{3+} ions are predominantly incorporated into Ca^{2+} positions. This site preference is consistent with previous reports on rare-earth-doped borate phosphors, where trivalent activators preferentially occupy divalent cation sites with local charge compensation. Such defect-assisted charge compensation mechanisms are likely to contribute to the formation of trapping centers responsible for the observed thermoluminescence behavior.

Although a secondary $Ca_3B_2O_6$ (takedaite) phase is present in a noticeable fraction, its contribution to the observed TL response cannot be strictly ruled out. However, available structural information and comparison with previously reported $NaCa_4(BO_3)_3$-based phosphor systems suggest that the dominant contribution is expected to originate from the $NaCa_4(BO_3)_3$ host lattice. To the authors' knowledge, no host-resolved TL data for $Ca_3B_2O_6$:Tb under comparable irradiation and readout conditions appear to be available in the accessible literature. A definitive quantitative separation of phase-specific TL contributions would require dedicated comparative samples or selective excitation studies, which are beyond the scope of the present work.

To further quantify the phase composition and structural parameters, Rietveld refinement was performed for the undoped and Tb^{3+}-doped samples, as shown in Fig. 1b. The refinement confirms that the samples consist predominantly of the $NaCa_4(BO_3)_3$ phase with a secondary $Ca_3B_2O_6$ phase. The obtained refinement parameters (χ^2, R_p, Rwp) indicate good agreement between the experimental and calculated patterns, confirming the reliability of the structural model. The presence of the secondary phase is attributed to the complex borate chemistry and synthesis conditions, and further optimization may be required to achieve phase-pure materials.

3.2. Band-pass filter-assisted thermoluminescence measurements

To investigate the spectral characteristics of the TL emission and to evaluate the contribution of different emission bands, TL measurements were performed using optical band-pass filters. These measurements were carried out on a representative Tb^{3+}-doped $NaCa_4(BO_3)_3$ sample ($Tb^{3+} = 0.5$ wt%), selected to provide sufficient TL signal intensity and spectral contrast for filter-based analysis. Band-pass filter experiments were not conducted for all Tb^{3+} concentrations, as the aim of this study was to obtain a qualitative assessment of wavelength-dependent TL sensitivity rather than a systematic concentration-dependent comparison. The TL signals were recorded using a set of optical filters centered at BSL-TL 365 nm, IRSL-TL 410 nm, and IRSL-TL 585 nm, selected to isolate specific emission bands while suppressing stimulation light, following common TL/OSL filtering strategies (Richter et al., 2015; Townsend, 1994; Niyonzima et al., 2024). The corresponding TL glow curves recorded with different band-pass filters are shown in Fig. 2. The 365 nm and 410 nm filters primarily sample the high-energy and blue emission components associated with host-related and Tb^{3+}-related transitions, respectively; in particular, the IRSL-TL 410 nm filter was chosen to selectively probe the blue Tb^{3+}-related emission while minimizing thermal background and overlap with the dominant green emission, whereas the 585 nm filter targets the dominant visible emission band commonly attributed to Tb^{3+} centers. This selection enables a qualitative comparison of wavelength-dependent TL contributions without requiring full spectral resolution. The measurements were performed under identical irradiation and heating conditions to ensure a reliable comparison between the filtered signals. In order to enhance the visibility of intensity variations over a wide dynamic range and to facilitate comparison between different spectral channels, the TL glow curves were displayed on a logarithmic intensity scale. This representation provides clear analytical advantages in luminescence sensitivity analysis, particularly for resolving low-intensity features and overlapping glow peaks, which aligns with the analytical advantages of logarithmic luminescence displays discussed by Can et al. (2025). The logarithmic display enables a more effective assessment of relative signal contributions across temperature regions that may otherwise be obscured in linear-scale representations. The filter-assisted TL measurements demonstrate that different spectral components contribute unequally to the overall glow curve shape and intensity distribution. These observations support the use of band-pass filters combined with logarithmic data representation as a practical approach for probing wavelength-dependent TL behavior in rare-earth-doped borate phosphors, in line with previous reports on filter-optimized TL detection.

3.3. Glow peak structure and concentration-dependent thermoluminescence response

The TL glow curve of the representative Tb^{3+}-doped $NaCa_4(BO_3)_3$ sample recorded under the IRSL-TL 410 nm filter exhibits a multi-peak

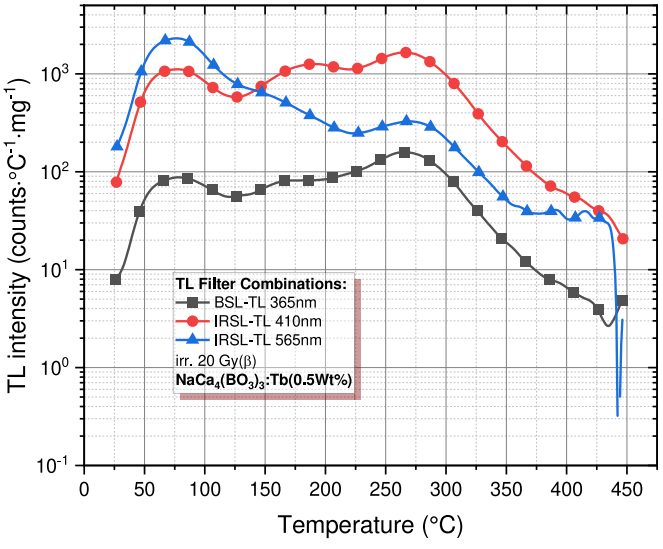

Fig. 2. Logarithmic TL glow curves of a representative Tb^{3+}-doped $NaCa_4(BO_3)_3$ sample (0.5 wt%) recorded using different band-pass filters.

structure, as shown in Fig. 3a. It should be noted that Rietveld refinement indicates the coexistence of a secondary $Ca_3B_2O_6$ (takedaita) phase in addition to the $NaCa_4(BO_3)_3$ host. All TL measurements were performed using a 410 nm detection window, which predominantly probes Tb^{3+}-related emission bands. Since Tb^{3+} ions are preferentially incorporated into the $NaCa_4(BO_3)_3$ lattice, the observed TL emission is mainly attributed to this phase. However, a minor contribution from the secondary phase cannot be strictly excluded. A rigorous separation of phase-specific TL contributions would require dedicated single-phase reference samples, which is beyond the scope of this study. Three distinct glow peaks are observed at approximately 77 °C, 188 °C, and 264 °C, indicating the presence of trapping centers with different thermal stabilities. The low-temperature peak around 77 °C is attributed to shallow traps that are thermally unstable, while the peak at about 188 °C is associated with traps of intermediate depth. The high-temperature peak located at approximately 264 °C corresponds to deeper and thermally more stable traps and is therefore of primary interest for reliable TL analysis.

In order to suppress the contributions from shallow and intermediate traps and to obtain a simplified TL response dominated by a single, stable glow peak, a preheating procedure was applied prior to TL readout. The influence of preheating temperature on the TL response was systematically investigated while keeping the preheating duration fixed at 7 s, and the results are presented in Fig. 3b. The preheating-temperature test demonstrates that increasing the preheating temperature effectively removes the low-temperature peak at 77 °C and fully suppresses the intermediate glow peak at 188 °C, whereas the high-temperature peak at 264 °C remains largely preserved. In the multi-peak TL glow curve shown in Fig. 3a, the glow peak around 188 °C is associated with traps of intermediate depth, which are fully suppressed by the applied preheating protocol. This behavior indicates that these traps are more sensitive to thermal treatment and therefore less suitable for stable and reproducible TL dosimetry. In contrast, the high-temperature glow peak at about 264 °C is related to deeper and thermally more stable traps and is thus considered the primary feature for reliable TL analysis. For this reason, in the present work the initial multi-peak glow curve is intentionally converted, by means of a controlled preheating step, into a simplified response governed by a single and well-resolved 264 °C peak, improving measurement reproducibility and reducing uncertainties in kinetic evaluation. This strategy is consistent with common practice in rare-earth-doped TL phosphors, where shallow and intermediate peaks are deliberately suppressed and only the stable peak in the 260–290 °C region is used for dosimetric analysis. The suppression of the 188 °C peak is motivated by its association with traps of intermediate thermal stability, which are more sensitive to thermal treatment and less suitable for stable and reproducible TL analysis. Such traps are prone to overlap with lower-temperature components and may introduce additional uncertainty in subsequent TL evaluations. In contrast, the 264 °C glow peak exhibits superior thermal stability and dominates the TL response after preheating, making it a more reliable feature for further analysis. Based on these observations, an appropriate preheating temperature was selected to eliminate the contributions of the shallow and intermediate traps without significantly affecting the high-temperature glow peak. This approach converts the initial multi-peak TL structure into a simplified response governed by a single, well-resolved glow peak at 264 °C, thereby improving measurement reproducibility and providing a robust basis for subsequent trap-related investigations. A similar preheating strategy, in which low- and

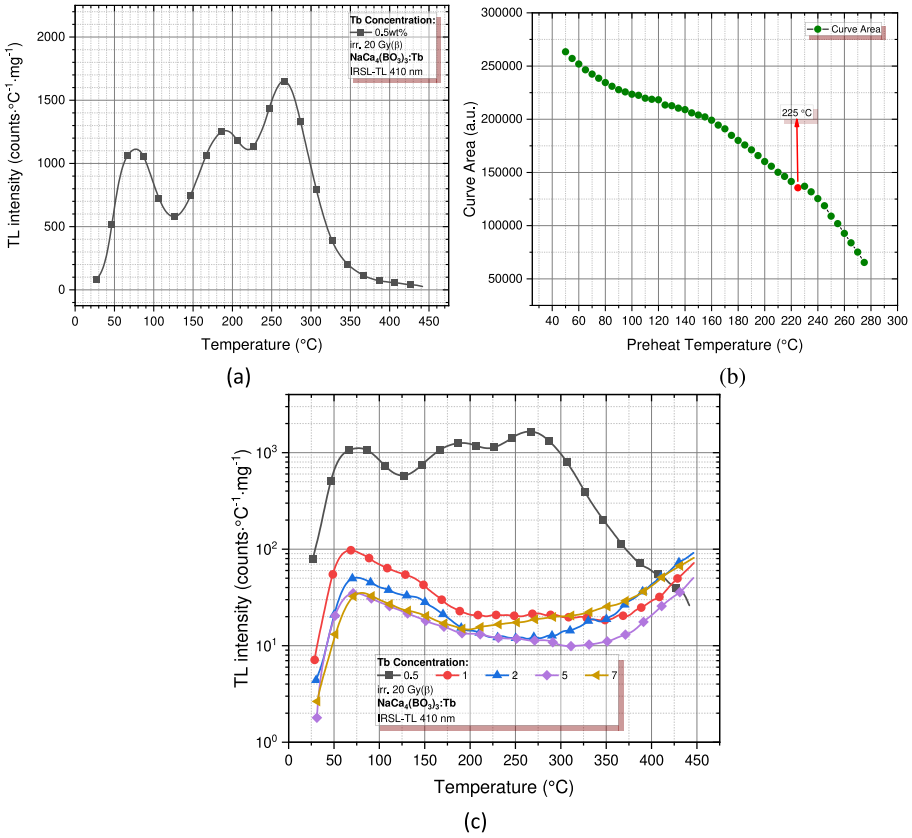

Fig. 3. (a) TL glow curve of the representative Tb^{3+}-doped $NaCa_4(BO_3)_3$ sample (0.5 wt%), showing multiple glow peaks associated with shallow, intermediate, and deep trapping levels. The presence of well-separated peaks at low (~77 °C), intermediate (~188 °C), and high (~264 °C) temperatures reflects a multi-trap structure with different thermal stabilities. (b) Dependence of TL curve area on preheating temperature for a fixed preheating duration of 7 s. (c) Logarithmic TL glow curves recorded at 410 nm for different Tb^{3+} concentrations. The TL intensity increases up to 0.5 wt% Tb^{3+} and decreases at higher concentrations, indicating concentration quenching due to enhanced non-radiative energy transfer between Tb^{3+} ions.

intermediate-temperature glow peaks are intentionally removed and a single high-temperature dosimetric peak is isolated, has been widely employed in rare-earth-doped TL phosphors such as Tb^{3+}-doped $LaCa_4O(BO_3)_3$, $LaB_3O_6:RE^{3+}$ and $KCaF_3:Tb^{3+}$, where shallow and intermediate traps are suppressed and only the stable peak around 260–290 °C is used for dosimetric analysis (Reddy et al., 2025; Portakal-Uçar et al., 2023; Keskin and İlhan, 2023; Madkhali et al., 2025).

Fig. 3c shows the TL glow curves recorded at 410 nm for different Tb^{3+} concentrations. The TL intensity reaches a maximum at 0.5 wt% Tb^{3+} and decreases at higher dopant concentrations, indicating concentration quenching. This behavior is characteristic of concentration quenching in rare-earth-doped TL and phosphor materials (Başaran et al., 2025; Kameshwaran et al., 2023).

At low Tb^{3+} concentrations, the number of efficient recombination centers increases, leading to enhanced TL emission. However, at higher dopant concentrations, reduced TL sensitivity is observed due to increased Tb^{3+}–Tb^{3+} interactions, which promote non-radiative energy transfer, cross-relaxation, and competitive recombination pathways, as commonly reported in Tb^{3+}-activated hosts (Ono et al., 2019; Kadari et al., 2013). As a result, a smaller fraction of the released charge carriers contributes to radiative recombination during thermal stimulation, leading to suppressed TL intensity. Lower Tb^{3+} concentrations below 0.5 wt% were not included in the present analysis, as the corresponding TL signals were found to be comparatively weak and less suitable for reliable filter-assisted and logarithmic-scale evaluation. The selected concentration range was sufficient to capture the characteristic trend of TL enhancement followed by concentration quenching (Madkhali et al., 2025; Gieszczyk et al., 2019).

3.4. Dose response and linearity characteristics

The dose-dependent TL behavior of the preheated Tb^{3+}-doped $NaCa_4(BO_3)_3$ sample (0.5 wt%) was investigated to evaluate its dosimetric response under β irradiation. Fig. 4a presents the TL glow curves recorded at 410 nm for irradiation doses ranging from 1.4 Gy to 501 Gy after applying a preheating treatment at 225 °C for 7 s. With increasing irradiation dose, a systematic enhancement in TL intensity is observed, while the glow curve shape and the position of the dominant peak at approximately 270 °C remain unchanged, indicating a stable trapping–recombination mechanism over the investigated dose range. The invariance of the dosimetric peak position (~264 °C) with increasing dose, together with the preserved peak shape, is characteristic of an effectively first-order–like kinetic regime (i.e., with negligible peak shift and minimal change in peak shape over dose), in agreement with previous studies on TL phosphors where non-shifting peaks were associated with first-order kinetics (Alajlani et al., 2021; Etefa et al., 2025). From a physical standpoint, kinetic simulations based on interactive multiple-trap system models indicate that the presence of several competing traps and recombination centers drives the main dosimetric peak toward a first-order shape and minimizes changes in peak

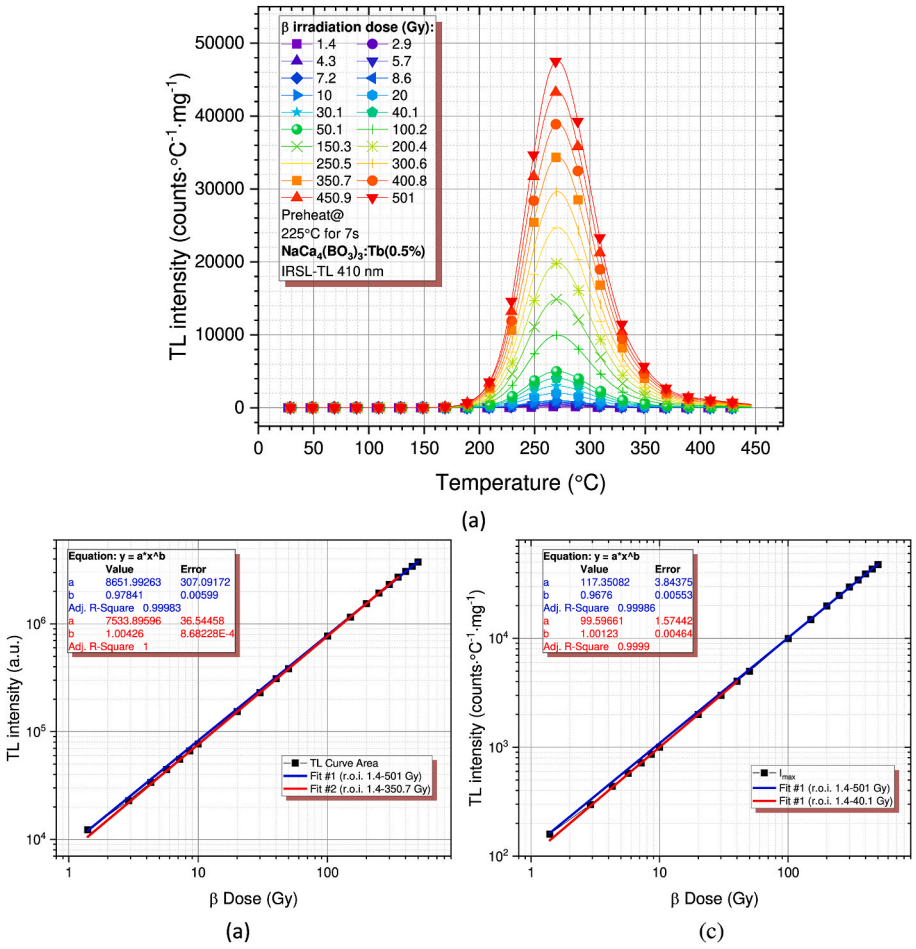

Fig. 4. (a) TL glow curves recorded at 410 nm for different β irradiation doses after preheating at 225 °C for 7 s. The TL intensity increases with dose while the peak position (~264–270 °C) remains nearly constant, indicating a stable dominant trapping center; slight broadening at low doses reflects contributions from shallow and intermediate traps. (b) Dose response based on the integrated TL curve area plotted on a logarithmic scale. The near-linear behaviour over a wide dose range confirms proportional dose dependence. (c) Dose response based on the maximum intensity of the isolated high-temperature glow peak. The agreement with area-based results supports the reliability of the peak as a dosimetric parameter.

temperature with dose (Pagonis and Kitis, 2012; Sadek et al., 2015; Pagonis et al., 2006). In such systems, a deep, thermally stable 'last' trap–recombination center pair dominates the recombination process and yields a dose-invariant dosimetric peak (Touliopoulos and Kitis, 2025). Similar behavior has been observed in rare-earth-doped borate and silicate hosts, where deep peaks in the 200–300 °C region show stable T_m and linear dose response over wide dose ranges, confirming their suitability for TL dosimetry (Anishia et al., 2010; Altowyan et al., 2024; Joseph et al., 2023; Reddy et al., 2025; Alajlani et al., 2021). The stable 270 °C peak in preheated Tb^{3+}-doped $NaCa_4(BO_3)_3$ can thus be attributed to a deep and thermally robust trapping–recombination system operating under effectively first–order–like conditions.

To quantify the dose response, two evaluation parameters were considered: the integrated TL curve area and the maximum intensity of the isolated high-temperature glow peak. Fig. 4b shows the dose dependence of the integrated TL curve area plotted on a logarithmic scale and fitted using a power-law relation $I = aD^b$. The fitted b-values obtained for two different dose intervals (1.4–50.1 Gy and 1.4–350.7 Gy) are found to be close to unity, demonstrating an approximately linear relationship between the integrated TL signal and the absorbed dose across these ranges. Fig. 4c displays the dose response derived from the maximum intensity of the 270 °C glow peak, which is regarded as the primary dosimetric parameter due to its association with deep and thermally stable traps. The peak-intensity-based dose response also follows a power-law behaviour with b-values very close to 1 for both evaluated dose intervals (1.4–50.1 Gy and 1.4–501 Gy), accompanied by high correlation coefficients. This confirms a linear TL response over a wide dose range and indicates that no significant supralinearity or saturation effects are present within the investigated doses.

Overall, the consistency of b-values close to unity obtained over low-to-intermediate and extended dose intervals provides strong evidence for a linear dose response behavior. This linearity, combined with the stability of the isolated high-temperature glow peak, highlights the suitability of the preheated Tb^{3+}-doped $NaCa_4(BO_3)_3$ phosphor for reliable TL dosimetric applications over a broad dose range.

3.5. Readout reproducibility and signal stability

The reproducibility and stability of the TL response were evaluated through successive readout cycles using the preheated Tb^{3+}-doped $NaCa_4(BO_3)_3$ sample (0.5 wt%). TL measurements were performed at 410 nm following a preheating treatment at 225 °C for 7 s, and the glow curves obtained from ten consecutive readout cycles are presented in Fig. 5a. The nearly overlapping glow curves demonstrate that repeated TL readout does not induce noticeable changes in the glow curve shape or peak position, indicating stable trap emptying and readout conditions (Oglakci et al., 2025; Guo et al., 2023).

For the reproducibility measurements, TL readouts were performed sequentially after β irradiation without intentionally imposing a fixed waiting time. However, due to the experimental procedure, the delay between irradiation and readout remained short and approximately consistent for all cycles, corresponding effectively to the early-time regime of the TL signal evolution.To quantitatively assess reproducibility, the maximum intensity of the isolated high-temperature glow peak was normalized to the first readout and plotted as a function of readout order, as shown in Fig. 5b. The normalized peak intensities remain close to unity throughout successive readouts, with all data points lying within the 95% confidence interval (Ngoc et al., 2025). This behavior confirms that the peak intensity exhibits high repeatability and

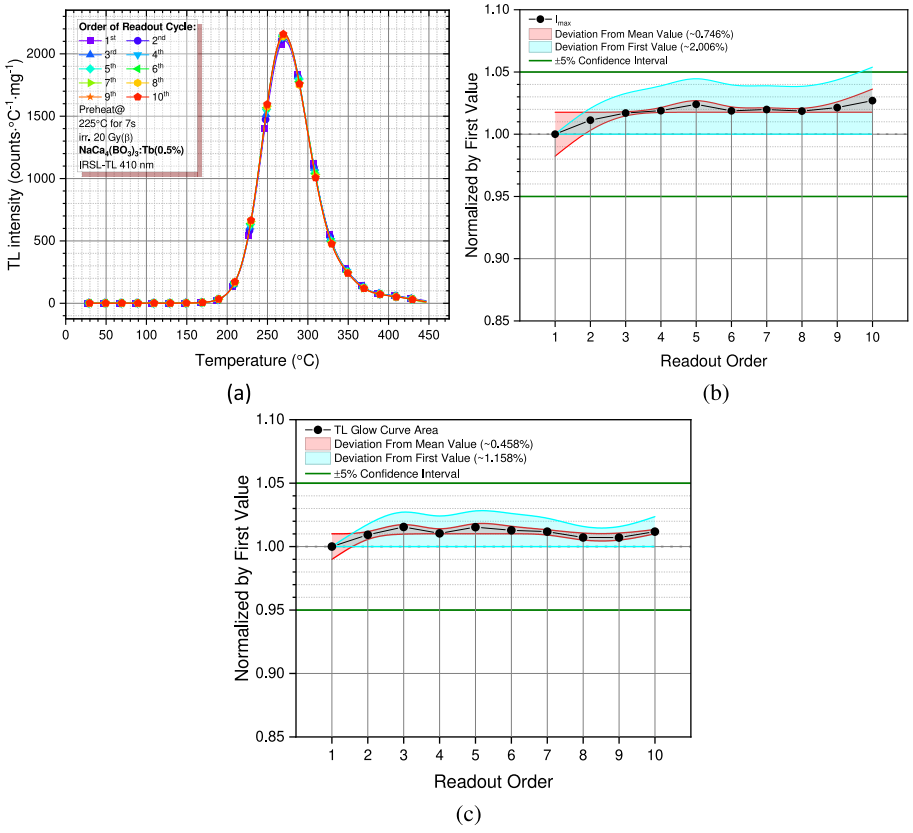

Fig. 5. (a) TL glow curves recorded at 410 nm for successive readout cycles after preheating at 225 °C for 7 s. The overall glow curve shape and peak position remain nearly unchanged over repeated cycles, indicating good reproducibility and thermal stability of the trapping system. (b) Normalized maximum glow peak intensity as a function of readout order. The small variation in intensity demonstrates stable signal retention with minimal degradation upon reuse. (c) Normalized integrated TL curve area as a function of readout order. The consistent response confirms the reusability of the material for repeated TL measurements.

that no significant signal degradation or sensitivity loss occurs during repeated TL measurements (Anishia et al., 2011). It should be noted that the reproducibility test reflects measurements performed under comparable short-delay conditions, prior to the onset of the pronounced time-dependent TL enhancement and delayed fading discussed in Section 5.In addition, the reproducibility of the TL response was examined using the normalized integrated TL curve area, presented in Fig. 5c. Similar to the peak-intensity analysis, the normalized TL curve area shows minimal variation with readout order and remains within the statistical confidence limits. The agreement between the peak-based and area-based evaluations further confirms the robustness of the TL readout process.

Overall, the excellent agreement observed for both the maximum glow peak intensity and the integrated TL curve area demonstrates that the preheated Tb^{3+}-doped $NaCa_4(BO_3)_3$ phosphor exhibits stable and repeatable TL readout behavior over successive cycles, comparable to established dosimetric phosphors (Oglakci et al., 2023, 2025; Ngoc et al., 2025). This high readout stability is essential for reliable TL dosimetric applications, particularly in repeated measurement, routine quality control, or calibration scenarios.

3.6. *Effect of heating rate on TL glow peak characteristics*

The influence of heating rate on the TL response of the preheated Tb^{3+}-doped $NaCa_4(BO_3)_3$ sample (0.5 wt%) was investigated to assess the kinetic stability and dosimetric reliability of the isolated high-temperature glow peak. TL glow curves were recorded at heating rates ranging from 0.1 to 10 °C s^{-1} after applying a preheating treatment at 225 °C for 7 s, as shown in Fig. 6a.

With increasing heating rate, the position of the dominant glow peak shifts systematically toward higher temperatures and the peak becomes progressively broader, in agreement with classical TL behaviour reported for many phosphors (Ahadova, 2024; Mammadov et al., 2024). Such behavior is characteristic of thermally stimulated processes and reflects the finite time available for charge carrier release and recombination at higher heating rates. Importantly, the overall glow curve shape remains well defined across the investigated heating rates, indicating that the TL response is governed by a single, kinetically stable trapping–recombination system rather than strongly overlapping peaks.

To further quantify the effect of heating rate, the normalized values of the peak temperature (T_m), maximum intensity (I_m), full width at half maximum (FWHM), and integrated TL curve area were evaluated, as presented in Fig. 6b. The peak temperature and FWHM increase monotonically with heating rate, whereas the normalized peak intensity

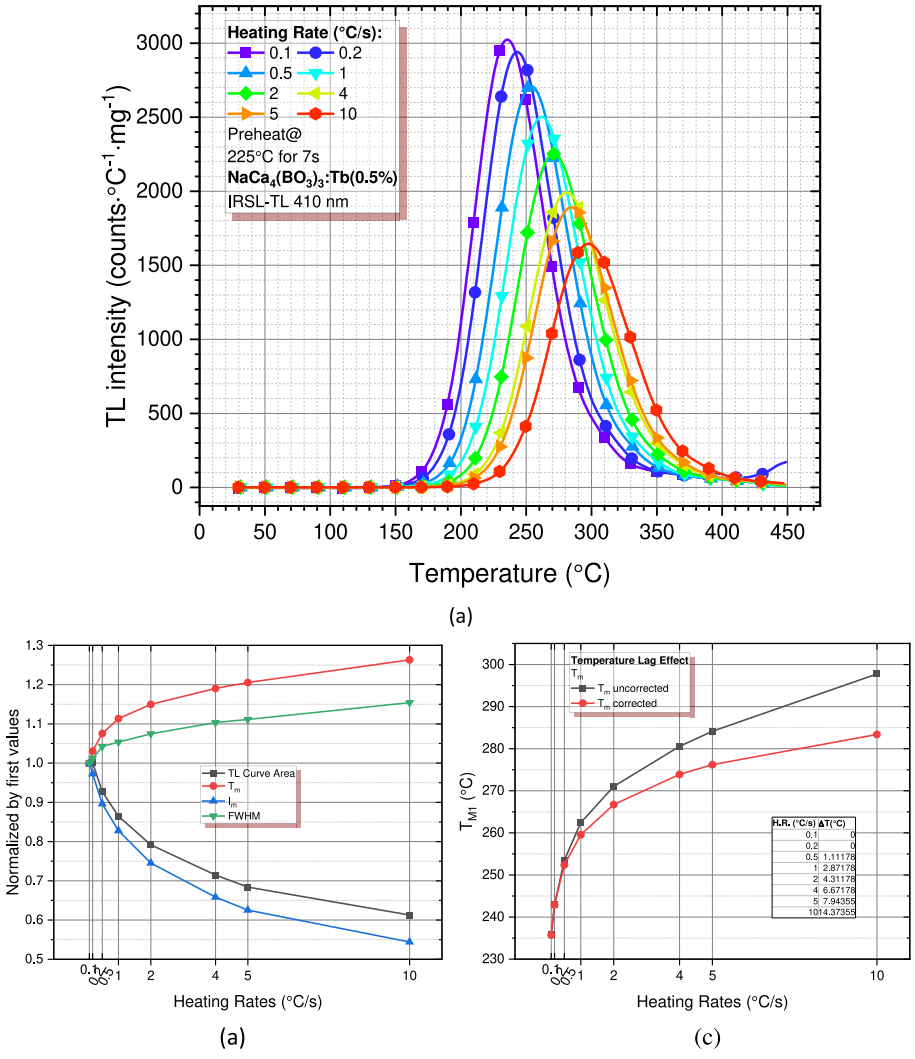

Fig. 6. Heating-rate effects on the isolated TL glow peak: (a) glow curves, showing a systematic shift of the peak towards higher temperatures with increasing heating rate, (b) normalized peak parameters, indicating changes in intensity and peak width due to thermal and kinetic effects, and (c) temperature-lag correction of T_m, demonstrating that the apparent peak shift is largely associated with thermal lag under fixed experimental conditions.

and TL curve area exhibit a systematic decrease, consistent with thermal quenching and intensity redistribution over a broader temperature interval (Kalita and Chithambo, 2017). This trend is consistent with classical TL kinetics and arises from the redistribution of emitted intensity over a broader temperature range at higher heating rates.

The observed heating-rate-dependent behavior supports the interpretation that the isolated high-temperature glow peak originates from deep and thermally stable traps and follows well-established TL kinetic principles. These results further confirm the suitability of the selected glow peak for reliable TL analysis and dosimetric evaluation under varying experimental conditions.

To account for the apparent shift of the glow peak temperature with increasing heating rate, the temperature lag effect was evaluated using a standard logarithmic correction approach (Delice, 2018; Kitis and Tuyn, 1998). The corrected peak temperature T_{m_j} corresponding to a heating rate βj was calculated relative to a reference heating rate β_i according to the relation:

$$T_{m_j} = T_{m_i} - \frac{T_{m_2} - T_{m_1}}{ln\left(\frac{\beta_2}{\beta_1}\right)} ln\left(\frac{\beta_i}{\beta_j}\right) \quad (1)$$

As shown in Fig. 6c, the corrected T_m values exhibit a significantly reduced dependence on heating rate compared to the uncorrected data, indicating that a substantial part of the observed peak shift arises from temperature lag rather than changes in trap kinetics. This correction demonstrates that the activation parameters of the high-temperature peak are effectively independent of heating rate, confirming the kinetic stability of the isolated trap and supporting its suitability for reliable TL analysis and dosimetric evaluation under varying readout conditions.

4. Kinetic parameters

4.1. Determination of kinetic parameters using heating-rate-based methods

The kinetic parameters associated with the dominant TL peak of $NaCa_4(BO_3)_3$:Tb were evaluated using heating-rate-based methods, namely the Hoogenstraaten variable heating rate (VHR) method and the Booth–Bohun–Parfianovitch (BBP) method. Using these two approaches in parallel allows a cross-check of the activation energy obtained from a global regression (VHR) with pairwise estimates (BBP), which is now common practice in TL kinetic analysis. These approaches, although introduced several decades ago, remain widely employed for the estimation of activation energy (E) and frequency factor (s) from the dependence of the glow peak temperature on the heating rate, and continue to provide reliable kinetic information in contemporary TL studies. The Hoogenstraaten VHR method is based on the analysis of the relationship between the peak temperature (T_m) and the heating rate (β), assuming first-order or quasi-first-order kinetics. By plotting ln (Tm^2/β) as a function of $1/(k_BTm)$, a linear relationship is obtained, from which the activation energy (E) is determined from the slope and the frequency factor (s) from the intercept. (Hoogenstraaten). The mathematical relations employed in this method have been described in detail in our previous studies (Coban et al., 2025). This method has been successfully applied in numerous TL investigations and is particularly useful when a single dominant glow peak can be clearly identified and separated from shallow components by an appropriate preheat protocol.

Fig. 7 illustrates representative VHR plots constructed using both uncorrected and temperature-lag-effect (TLA)-corrected peak temperatures. In both cases, a high degree of linearity is observed, indicating that the heating-rate dependence of the peak temperature is well described by the Hoogenstraaten formalism. However, correction for temperature lag following a logarithmic scheme similar to Delice (2018) reduces the apparent shift of T_m with β and tightens the regression,

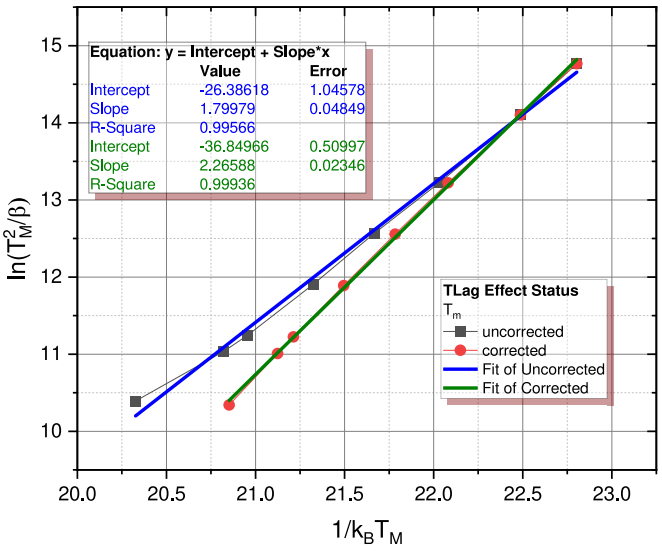

Fig. 7. Representative plots used for the determination of kinetic parameters by the Hoogenstraaten variable heating rate (VHR) method, constructed using uncorrected and thermal-lag–corrected peak temperatures (T_m).

leading to more robust values of E and s. In particular, the use of TLA-corrected T_m values leads to improve linear fits and reduced scatter, showing that a significant part of the raw T_m shift arises from instrumental lag rather than genuine kinetic changes. In parallel, the Booth–Bohun–Parfianovitch method was employed as an independent means of estimating the activation energy. This approach utilizes pairs of heating rates and their corresponding peak temperatures and is expressed by the well-known BBP equation, which relates E to the logarithmic ratio of heating rates and peak temperatures. The BBP method has historically played an important role in TL kinetic analysis (Booth, 1954; Bohun, 1954; Parfianovitch, 1954) and remains valuable today mainly as a cross-validation tool for regression-based methods such as VHR, especially when only a limited set of heating rates is available. Activation energies derived from the BBP analysis for different heating-rate pairs are summarized in Table 1, together with the corresponding values obtained from the Hoogenstraaten method. Activation energies derived from the BBP analysis for different heating-rate pairs are summarized in Table 1, together with the corresponding values obtained from the Hoogenstraaten method. For the uncorrected dataset, the VHR parameters ($E = 1.80 \pm 0.04$ eV, $s = 6.01 \times 10^{15}$ s^{-1}) are internally consistent with the first-order peak-maximum condition within the expected uncertainty range, and therefore provide the most reliable effective kinetic description of the dominant TL peak. In

Table 1
Activation energies (E) and frequency factors (s) obtained using the Booth–Bohun–Parfianovitch (BBP) and Hoogenstraaten (VHR) methods for uncorrected and thermal-lag–corrected peak temperatures at different heating rates.

β (°C/s)	*Maximum 1*		
	UnCorrecred	*Corrected*	
0.2	2.09	2.09	Booth-Bohun-Parfianovitch
0.5	2.01	2.14	Method
1	1.94	2.17	
2	1.93	2.19	
4	1.91	2.23	
5	1.88	2.24	
10	1.77	2.27	
Average E (eV)	**1.93 ± 0.1**	**2.19 ± 0.06**	
***E* (eV) (0.2–10 °C/s)**	1.80 ± 0.04	2.26 ± 0.02	Hoogenstraaten's Method
***s* (s^{-1})**	$6.01x10^{15}$	$2.65x10^{11}$	

contrast, the parameter combination obtained after applying the temperature-lag correction ($E = 2.26 \pm 0.02$ eV, $s = 2.65 \times 10^{11}$ s^{-1}) does not satisfy the first-order maximum condition for the experimental T_m and β values, indicating that the correction overcompensates the apparent peak shift. This interpretation is further supported by the monotonic increase of BBP-derived activation energies with heating rate in the corrected dataset, which is not expected for an isolated first-order peak. Therefore, the temperature-lag-corrected kinetic parameters are retained only for qualitative illustration of the instrumental lag effect and are not used for further quantitative kinetic interpretation. For both uncorrected and corrected datasets, the BBP-derived activation energies exhibit good internal consistency and are in reasonable agreement with those obtained from the VHR analysis, yielding effective activation energies in the range of approximately ~1.9 eV (uncorrected) to ~2.2–2.3 eV (corrected). Notably, the corrected values display a reduced spread (e.g., ±0.06 eV compared to ±0.10 eV for the uncorrected case), indicating that thermal lag correction improves the robustness and internal consistency of the extracted kinetic parameters.

The frequency factors calculated using the Hoogenstraaten method are also listed in Table 1. As commonly observed in TL studies, the values of *s* are sensitive to both the assumed kinetic model and the accuracy of the peak temperature determination. Nevertheless, the TLA-corrected dataset yields frequency factors in the range $s \approx 10^{11}$–10^{15} s^{-1}, which falls within a physically reasonable interval for deep, dosimetric TL peaks in oxide and borate hosts and is comparable to values reported for other rare-earth-doped borate phosphors. This agreement in the order of magnitude of *s* further supports the physical plausibility of the derived kinetic parameters.

It is important to emphasize that, given the complexity of the glow curve and the possibility of multiple contributing traps, the kinetic parameters obtained in this section should be regarded as effective parameters associated with the dominant TL peak, rather than as descriptors of individual trapping levels. This interpretation is consistent with modern multi-trap models (e.g. interactive multiple-trap system and competition-based approaches), which show that a composite trap network can still produce an apparently first-order-like peak with well-defined effective *E* and *s*. A more detailed discussion of the underlying trap structure and its implications, based on T_M-T_{stop}, Initial Rise, and deconvolution analyses, is presented in the subsequent sections.

Overall, the combined use of the Hoogenstraaten and Booth–Bohun–Parfianovitch methods provides a consistent and mutually cross-validated quantitative description of the kinetic behavior of the main TL peak in $NaCa_4(BO_3)_3$:Tb. The convergence of *E* values from both heating-rate-based approaches, together with the improvement after temperature-lag correction, supports the reliability of the extracted activation energies and frequency factors and establishes a solid foundation for the more detailed trap-structure analysis that follows.

It should also be noted that in the presence of unresolved overlapping components, heating-rate-based methods may yield activation energies that reflect the dominant rate-controlling sub-component rather than a single isolated trapping level.

4.2. T_M–T_{stop} and Initial Rise analysis: effect of preheating on trap structure

To further elucidate the trap structure responsible for the complex, multi-component TL behavior of $NaCa_4(BO_3)_3$:Tb, the T_M–T_{stop} technique combined with the Initial Rise (IR) method was employed. This combined protocol is widely used to resolve overlapping TL peaks and to estimate activation energies even when the glow curve is broad or composite (Alajlani et al., 2021; Sadek et al., 2015; Benavente et al., 2020; Gavhane et al., 2020). Such methods are particularly valuable in rare-earth-doped borate and silicate phosphors, where several trapping levels frequently contribute to nominally single glow peaks (Oglakci et al., 2023; Sonsuz et al., 2022). In the present case, the joint T_M–T_{stop}–IR analysis already suggests that $NaCa_4(BO_3)_3$:Tb does not behave as a simple single-trap system, but rather exhibits a quasi-continuous or closely spaced distribution of trapping levels, in line with earlier reports on complex defect landscapes in rare-earth-activated borates and silicates (e.g., TL analyses of multi trap systems in borate matrices and continuous trap distributions in $YAl_3(BO_3)_4:Sm^{3+}$ and $LaCa_4O(BO_3)_3:Tb^{3+}$) (Madkhali et al., 2025; Altowyan et al., 2023).

Fig. 8a shows the TL glow curves obtained using the T_M–T_{stop} protocol without any preheating treatment. A progressive evolution of the glow curve shape is observed as the stopping temperature (T_{stop}) increases, indicating the presence of multiple overlapping TL components rather than a single discrete peak. The corresponding T_M versus T_{stop} plot (Fig. 8b) reveals a continuous upward shift of the glow peak maximum with increasing Tstop. This systematic T_M shift is fully consistent with the classical T_M–T_{stop} behavior predicted for overlapping first-order peaks, as described in McKeever's foundational treatment of TL kinetics (McKeever, 1980). In such systems, progressive emptying of shallower traps at successive T_{stop} values leads to preferential observation of deeper components, causing T_M to move steadily to higher temperatures. The behavior observed in Fig. 8b therefore provides strong evidence for a hierarchy of traps with different thermal stabilities that compete for charge carriers. Such behavior is characteristic of a quasi-continuous or closely spaced distribution of trapping levels, suggesting that charge storage in this material is governed by a complex defect landscape similar to that interfered for $LaBO_3:Eu^{3+}$, $YAl_3(BO_3)_4:Sm^{3+}$ and $Li_2B_4O_7$:Cu,Ag (Benavente et al., 2020; Sonsuz et al., 2022; Altowyan et al., 2023).

To gain further insight into the energetic structure of these traps, the Initial Rise method was applied to the partial glow curves extracted from the T_M–T_{stop} measurements. The resulting activation energies as a function of T_{stop} are presented in Fig. 8c. In the absence of preheating, the estimated trap depths exhibit a step-like progression, allowing the identification of multiple trapping components distributed over a wide energy range, spanning approximately 0.9–1.1 eV for shallow traps, 1.2–1.4 eV for intermediate components, and extending up to ~1.6–1.7 eV for deeper trapping states. The step-like evolution was segmented into 13 plateaus by grouping consecutive IR-derived activation energies that fall within their typical uncertainty range ($\Delta E_{IR} \approx \pm 0.05$–$0.08$ eV) and do not exhibit a systematic trend with increasing T_{stop}. Individual error bars are not shown to maintain figure readability; however, the quoted uncertainty range reflects the typical fitting variability of the IR method under these conditions. It should also be noted that some adjacent plateaus are nearly indistinguishable within these uncertainty margins. Therefore, the step-like representation should be interpreted as a convenient visualization of a quasi-continuous distribution of trapping levels rather than as evidence for sharply separated discrete levels. Such 'energy staircase' behavior in IR-derived activation energies, involving discrete increases from shallow (~1.0 eV) to deeper (~1.6 eV) traps, has been reported in other borate-based dosimetric materials and is typically interpreted as a signature of a multi-trap–single-luminescence-center (MTSLC) system, where one dominant recombination center is coupled to several distinct trapping groups. In $NaCa_4(BO_3)_3$:Tb, the combined experimental results are consistent with Tb^{3+} acting as the primary recombination center, while a distributed set of intrinsic defects (e.g., cation vacancies and borate network defects) and extrinsic defects provides the trapping sites, in line with interpretations reported for rare-earth-doped borates and aluminates based on combined IR and glow-curve deconvolution analyses. For each partial glow curve, the Initial Rise (IR) fits were restricted to the low-temperature leading edge, corresponding to approximately the first 10–15% of the maximum TL intensity for the respective Tstop value. This range is consistent with the standard validity domain of the IR method. Because the glow curve consists of multiple overlapping components, the selected initial-rise region at a given Tstop may still include minor contributions from preceding peaks. Therefore, the IR-derived activation energies should be regarded as effective values representing groups of nearby traps rather than strictly isolated trapping levels.

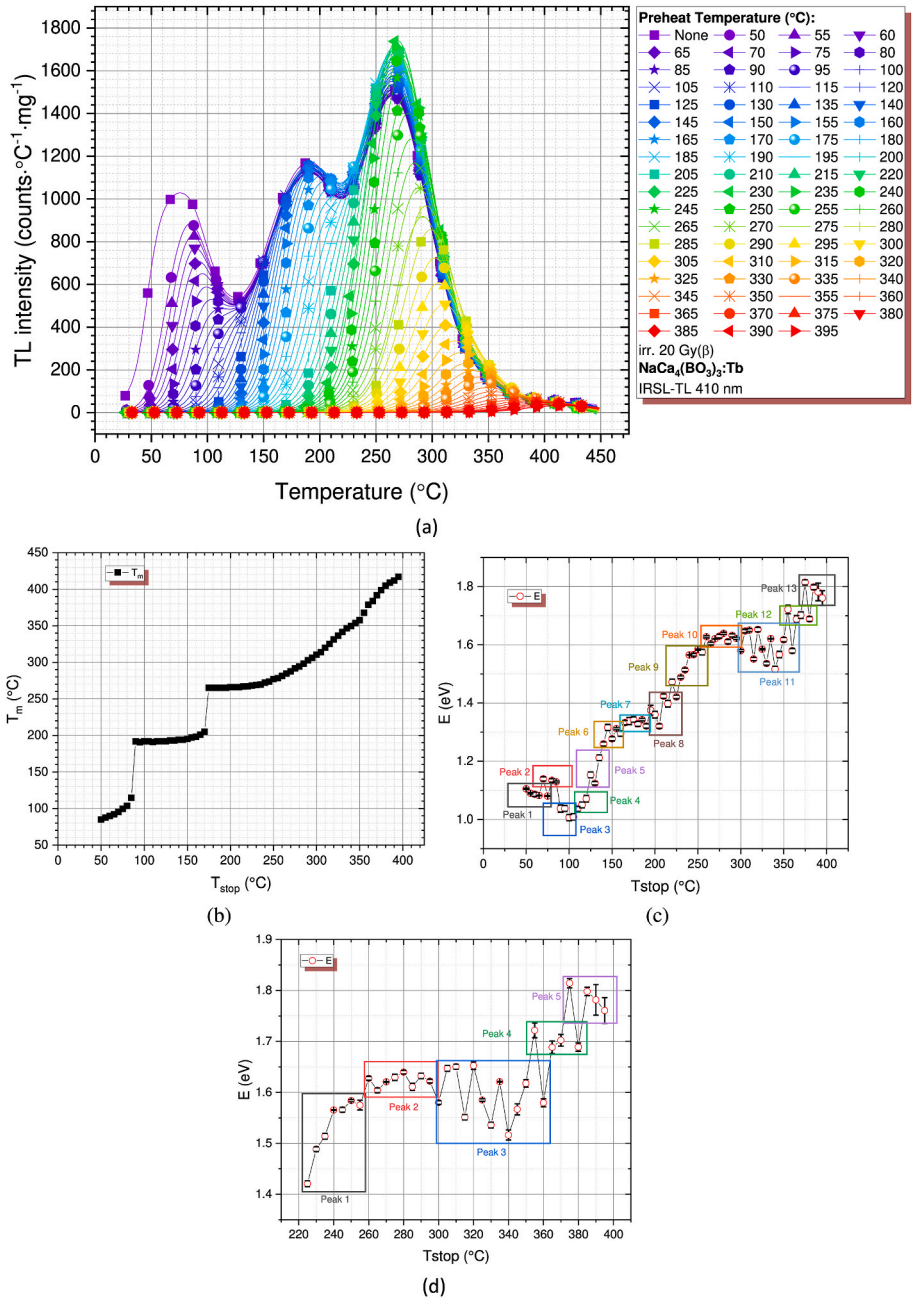

Fig. 8. (a) TL glow curves obtained using the T_M–T_{stop} technique without preheating, recorded at different stopping temperatures (T_{stop}), showing the evolution of the glow curve shape and intensity. (b) Corresponding T_M versus T_{stop} plot derived from the data in (a), indicating a continuous shift of the glow peak maximum with increasing T_{stop}. (c) Activation energies determined by the Initial Rise (IR) method as a function of T_{stop} for the non-preheated sample, revealing multiple overlapping trapping components. (d) Activation energies obtained from IR analysis after preheating, showing a reduced number of energetically distinct trapping levels and improved separation of deeper traps.

Because the glow curve consists of multiple overlapping components, the selected initial-rise region at a given Tstop may still include minor contributions from preceding peaks. Therefore, the IR-derived activation energies should be regarded as effective values representing groups of nearby traps rather than strictly isolated trapping levels.This behavior confirms that the apparent single dominant glow peak is, in fact, composed of several overlapping contributions with different thermal stabilities. Taken together with the T_M–T_{stop} evolution, the IR results strongly support the view that $NaCa_4(BO_3)_3$:Tb possesses a quasi-continuous trap distribution rather than well-separated, isolated levels, which is consistent with contemporary models of defect clustering and charge-compensating complexes in complex borate hosts and with continuous trap-depth ranges reported for Y_2MgTiO_6:Tm^{3+},Dy^{3+} (Wang et al., 2025).

In order to suppress the influence of shallow traps and clarify the contribution of deeper trapping states, an additional set of T_M–T_{stop} measurements was performed after applying a suitable preheating treatment. The corresponding activation energies derived from the IR analysis are shown in Fig. 8d. Compared to the non-preheated case, the preheated sample exhibits a reduced number of energetically distinct components, with clearer separation between individual trap groups, and activation energies predominantly confined to a deeper range of approximately 1.4–1.7 eV, while shallow traps below ~1.1 eV are strongly suppressed or no longer detectable. This indicates that

preheating effectively removes unstable shallow traps, thereby enhancing the visibility of deeper and more thermally stable trapping levels. This kind of thermal cleaning behavior is in good agreement with observations in other Tb- or Eu-doped borate and aluminate phosphors, where controlled preheating has been used to suppress fast-fading components and to isolate more dosimetrically useful, thermally robust peaks (see, for example, recent TL studies on rare-earth-doped borate dosimeters that optimize preheat conditions for stabilizing the main dosimetric peak).

The comparison between non-preheated and preheated T_M–T_{stop} runs in $NaCa_4(BO_3)_3$:Tb is therefore physically very informative. Removal of shallow, metastable traps (with activation energies below ~1.1 eV) simplifies the effective trap spectrum and isolates a smaller number of deeper components (predominantly above ~1.4 eV), as directly evidenced by the IR-derived activation energies shown in Fig. 8c and d. This trend is consistent with the depletion of thermally unstable levels responsible for rapid fading or delayed charge transfer. Similar protocol-dependent simplifications of glow-curve structure have been documented in commercial dosimetric materials such as LiF:Mg,Ti and LiF:Mg,Cu,P, where a preheat stage is routinely implemented to clean unstable traps before reading the main peak (see, e.g., recent optimization studies on LiF-based TL dosimeters for medical and environmental dosimetry) and in model analyses of competing deep and shallow traps in persistent phosphors (Pagonis and Kitis, 2012; Van der Heggen et al., 2020).

The comparison between preheated and non-preheated conditions demonstrates that the TL response of $NaCa_4(BO_3)_3$:Tb is strongly influenced by shallow, metastable traps that contribute to the overall glow curve complexity. The presence of these traps is consistent with the previously observed anomalous time-dependent TL enhancement, as such metastable states can participate in delayed charge redistribution processes prior to TL readout. The T_M–T_{stop} and IR analyses therefore provide independent experimental evidence supporting a multi-trap system with significant trap competition and redistribution dynamics. From a physical point of view, this implies that charge carriers initially stored in shallow traps can thermally migrate to deeper, more stable traps during storage, leading to post-irradiation TL build-up (anti-fading) and non-monotonic fading curves, phenomena that have been systematically discussed in the context of complex trap networks and thermally assisted charge transfer in TL phosphors.

Overall, the combined T_M–T_{stop} and Initial Rise analyses confirm that the TL glow curve of $NaCa_4(BO_3)_3$:Tb arises from multiple overlapping trapping levels with varying thermal stabilities. This multi-trap architecture has two important and partly opposing dosimetric implications. On one hand, metastable shallow traps can induce time-dependent signal evolution and complicate straightforward dose reconstruction. On the other hand, the deeper, thermally robust traps isolated after an appropriate preheating protocol may offer a stable dosimetric signal, provided that the readout procedure explicitly includes a standardized preheat stage to empty unstable levels. This kind of “protocol-engineered” stabilization of the main dosimetric peak is fully consistent with best practices in modern TL dosimetry and aligns well with McKeever's theoretical framework for analyzing and optimizing composite glow curves in multi-trap systems. The combined T_M–T_{stop} and IR analyses support a multi-trap single-luminescence-center (MTSLC) scenario, in which multiple trapping levels feed a dominant recombination center. In this framework, each individual CGCD component can be interpreted as an effective one-trap–one-recombination-center (OTOR-type) contribution with near-first-order kinetics, embedded within a competitive multi-trap network. Accordingly, the use of the GOK formalism should be regarded primarily as a numerical fitting tool for representing peak shapes, rather than as evidence for genuine general-order kinetics.In summary, the T_M–T_{stop} and IR results for $NaCa_4(BO_3)_3$:Tb are in good agreement with the current understanding of complex trap systems in rare-earth-activated borate phosphors: they point to a quasi-continuous trap spectrum coupled to a single dominant recombination center, strong trap competition and charge redistribution, and a decisive role of shallow metastable traps in governing fading, anti-fading, and the overall dosimetric performance of the material.

4.3. Computerized glow curve deconvolution (CGCD) analysis

In TL materials, overlapping glow peaks commonly arise from the presence of multiple trapping levels, making conventional peak position analysis inadequate. To separate the individual components contributing to the TL glow curves of $NaCa_4(BO_3)_3$:Tb, computerized glow curve deconvolution (CGCD) was employed, allowing the composite signal to be resolved into constituent peaks associated with distinct trapping levels.

In the present work, the CGCD analysis was performed using the *tgcd* package implemented in the R statistical computing environment, an open-source software specifically developed for TL glow curve analysis. The deconvolution procedure was carried out assuming general-order kinetics (GOK), which provides sufficient flexibility to describe TL peaks that deviate from ideal first- or second-order behavior. The analytical expression used to model the individual glow peaks is given by Eq. (2) (Peng et al., 2016):

$$I(T) = I_m \exp\left(\frac{E}{kT_m^2}(T - T_m)\right)\left[\frac{1}{b} + \frac{b-1}{b}\exp\left(\frac{E}{kT_m^2}(T - T_m)\right)\right]^{-\frac{b}{b-1}} \quad (2)$$

where I_m and T_m denote the maximum intensity and peak temperature, respectively, E is the activation energy, b is the kinetic order, and k is the Boltzmann constant. Equation (2) represents a commonly used simplified form of the general-order kinetics (GOK) expression derived from the full Kitis–Gómez-Ros–Tuyn formalism (Kitis et al., 1998), in which correction factors such as $\Delta = 2\ kT/E$ and $Z_m = 1 + (b - 1)\ \Delta_m$ are neglected. This simplification introduces a systematic bias, particularly for low-temperature and low-activation-energy peaks where the term $2kT_m/E$ is not negligible. In the present work, Eq. (2) is employed as a practical and widely used shape function for phenomenological glow curve deconvolution. Therefore, the extracted kinetic parameters should be regarded as effective values with method-dependent systematic uncertainties, especially for shallow trapping components. The use of the full formalism would be expected to slightly modify the extracted parameters for low-temperature peaks but would not alter the overall interpretation of a multi-trap system.

Computerized glow curve deconvolution was applied in conjunction with the E versus T_{stop} analysis in order to examine the effect of preheating on the effective glow curve structure. The results obtained before preheating are presented in Fig. 9a, which shows the evolution of activation energy as a function of T_{stop}, together with the corresponding CGCD fit of the TL glow curve in Fig. 9b. In this case, an adequate reproduction of the experimental glow curve requires a relatively large number of individual components, reflecting a complex superposition of trapping levels. The deconvolution results summarized in Table 2 indicate that the activation energies are broadly distributed, spanning approximately ~1.0 to ~1.8 eV, with more than ten partially overlapping peak components contributing to the overall TL emission.

After applying the preheating treatment, a markedly different behavior is observed. The post-preheating E versus T_{stop} results shown in Fig. 9c, together with the corresponding CGCD analysis in Fig. 9d, reveal a substantially simplified glow curve structure. In this case, the TL glow curve can be satisfactorily described using a much smaller number of components. As summarized in Table 3, the extracted activation energies after preheating are predominantly confined to a narrower and deeper range, typically between ~1.5 and ~1.8 eV, with only a few well-resolved peaks required to reproduce the experimental data. The activation energy ranges obtained from T_M–T_{stop}/IR and CGCD analyses are mutually consistent within the expected methodological uncertainties.

The CGCD fits yield kinetic orders in the narrow range $b \approx 1.01$–1.17 for all components before and after preheating (Tables 2 and 3),

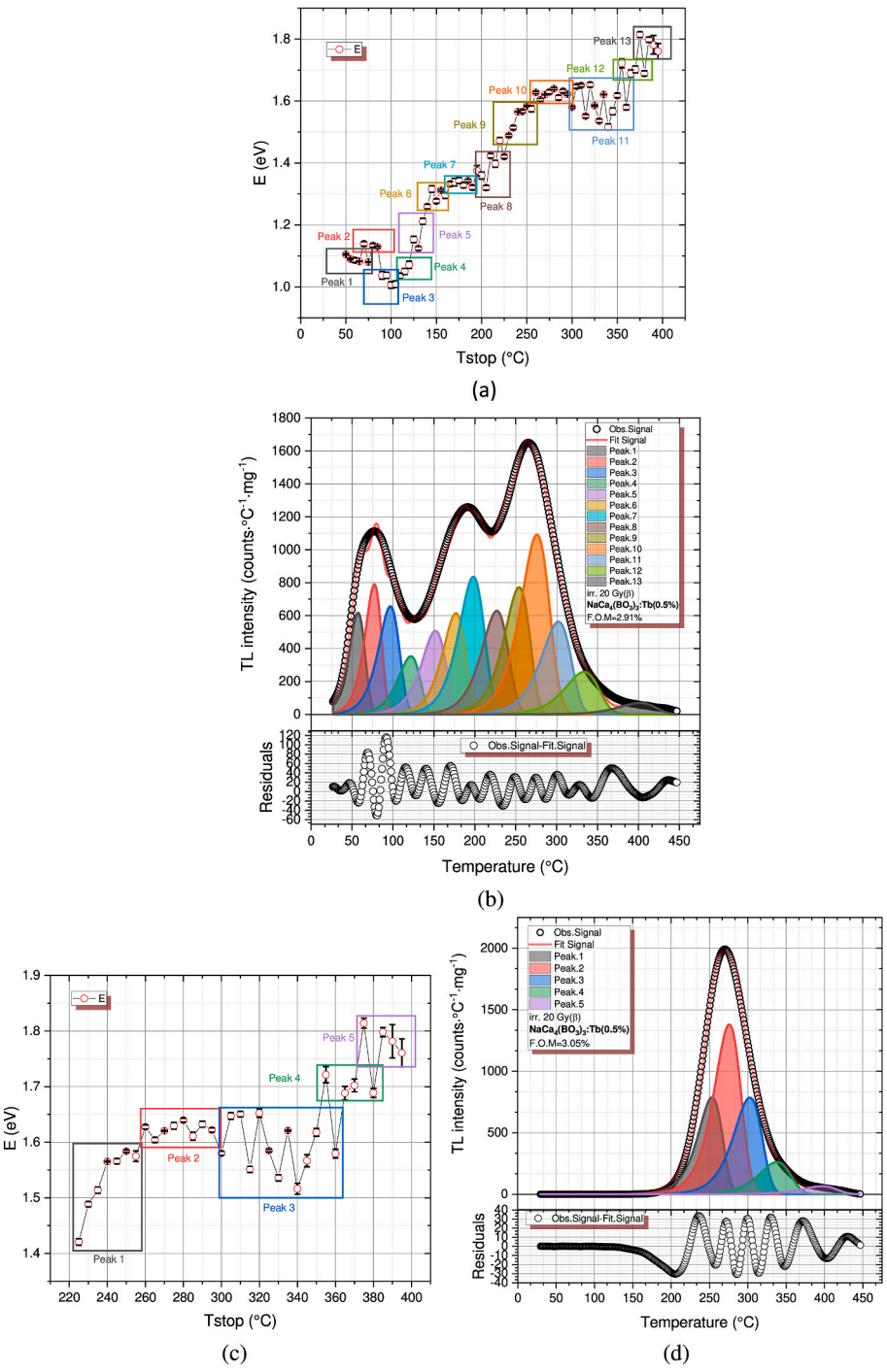

Fig. 9. (a) Activation energy (E) as a function of stopping temperature (T_{stop}) before preheating, showing a continuous distribution of trap energies associated with shallow and intermediate traps. (b) Corresponding CGCD analysis of the TL glow curve before preheating, revealing multiple overlapping components. (c) Activation energy (E) versus T_{stop} after preheating, indicating the suppression of shallow traps and the dominance of deeper trapping levels. (d) CGCD analysis of the TL glow curve after preheating, showing a reduced number of components and a simplified trap structure dominated by thermally stable traps.

indicating effectively first-order-like behavior of the resolved peaks. In this quasi-first-order regime, the χ^2 surface becomes relatively flat along the b-direction and the kinetic order is not tightly constrained by the data. Consequently, the parameter b should be regarded as a weakly determined shape parameter rather than an independently meaningful kinetic observable. Test fits performed using pure first-order kinetics ($b = 1$) for all components produced FOM values and residuals comparable to those of the GOK fits, indicating that allowing b to vary does not significantly improve the fit quality. Therefore, the deconvoluted peaks can be effectively treated as first-order components. This is also consistent with the measured symmetry factors ($\mu \approx 0.40$–0.43), which are characteristic of first-order TL peaks.

The quality of the deconvolution in both cases was evaluated using the figure-of-merit (FOM) values and residual analysis, confirming that the fitted curves provide a satisfactory representation of the measured TL glow curves. The comparison between Fig. 9b and d clearly demonstrates that preheating suppresses shallow and thermally unstable components, leading to a reduction in peak overlap and improved separation of the remaining trapping levels. The number of deconvolution components was determined using a combined approach based on

Table 2
CGCD-derived kinetic parameters (activation energy EEE, kinetic order b, and frequency factor *s*) obtained from the TL glow curve before preheating.

•	E_a (eV)	*b*	T_m (°C)	T_{m1} (°C)	T_{m2} (°C)	μ	*s* (s^{-1})
1st Peak	1.08	1.17	57.3341	44.045	67.1499	0.409	6.71×10^{15}
2nd Peak	1.13	1.09	77.3209	63.3038	87.2569	0.39899	3.77×10^{15}
3rd Peak	1.00	1.12	96.85	79.0822	109.6466	0.42359	7.02×10^{12}
4th Peak	1.03	1.01	121.85	102.7247	134.8211	0.4088	2.12×10^{12}
5th Peak	1.12	1.08	151.85	131.1216	166.4682	0.41781	2.73×10^{12}
6th Peak	1.31	1.06	176.85	157.0795	190.6407	0.41538	7.01×10^{13}
7th Peak	1.34	1.13	198.1218	176.5571	213.7345	0.4313	2.96×10^{13}
8th Peak	1.42	1.11	226.85	204.0575	243.1833	0.42129	2.69×10^{13}
9th Peak	1.58	1.02	254.0653	231.7915	269.2581	0.41525	1.67×10^{14}
10th Peak	1.63	1.15	275.9098	251.7419	293.5885	0.42748	1.13×10^{14}
11th Peak	1.65	1.05	302.1866	276.5895	319.9448	0.42082	3.27×10^{13}
12th Peak	1.68	1.14	333.3933	304.8424	354.1728	0.41501	9.56×10^{12}
13th Peak	1.81	1.04	401.85	369.8227	423.9472	0.41104	3.01×10^{12}

Table 3
CGCD-derived kinetic parameters (activation energy E, kinetic order *b*, and frequency factor *s*) obtained from the TL glow curve after preheating.

•	E_a (eV)	*b*	T_m (°C)	T_{m1} (°C)	T_{m2} (°C)	μ	*s* (s^{-1})
1st Peak	1.58	1.05	253.5221	231.1254	269.06	0.40491	1.73×10^{14}
2nd Peak	1.63	1.14	275.9242	251.8101	293.4744	0.42661	1.13×10^{14}
3rd Peak	1.65	1.08	302.6838	276.8587	320.8986	0.41323	3.17×10^{13}
4th Peak	1.72	1.13	337.85	309.6208	358.2916	0.42308	1.63×10^{13}
5th Peak	1.81	1.06	396.85	365.1347	418.9761	0.41374	3.84×10^{12}

guidance from T_M–T_{stop} and IR analyses, together with iterative fitting using FOM minimization and residual evaluation to ensure physically meaningful results and to avoid overfitting.

In the pre-preheating case, an adequate reproduction of the experimental glow curve required 13 GOK components, yielding a FOM value of 2.91%. We note that such a large number of free parameters implies that the solution is not mathematically unique. In this work, the number of components was guided by independent T_M–T_{stop} and Initial Rise analyses and was increased iteratively until the FOM reached a stable plateau and the residuals no longer exhibited systematic structure. Fits using fewer components resulted in structured residuals and significantly higher FOM values (>∼5%), indicating underfitting of the strongly overlapping glow peaks. Therefore, the 13-component solution is used here as a phenomenological description of a complex multi-trap system rather than as evidence for 13 discrete trapping levels. A rigorous model selection using information criteria (e.g., AIC, BIC) and a systematic exploration of alternative kinetic models, as well as metrological uncertainty quantification (including covariance propagation and Monte Carlo validation), have recently been emphasized in open-source TL analysis frameworks (Romero et al., 2026). Such a comprehensive analysis is beyond the scope of the present study and will be addressed in future work.

It should be emphasized that the CGCD results presented here provide an effective, phenomenological description of the glow curve structure under different thermal histories, rather than one-to-one representations of individual physical traps. A more detailed physical interpretation of the extracted activation energies and their correlation with the underlying trap distribution, including their relationship with the T_M–T_{stop} and Initial Rise analyses, is discussed in the subsequent sections. Although the CGCD peaks should be regarded as effective, phenomenological components rather than one-to-one representations of individual traps, and mechanisms such as trap–center competition, tunneling-mediated charge transfer, and interactions with deep or non-radiative competitors may also modulate the apparent glow-curve structure; the combined T_M–T_{stop}/IR and CGCD results consistently indicate that the dominant effect of the preheating protocol is the thermal cleaning of shallow, metastable traps and the isolation of a smaller set of deeper, dosimetrically useful levels. Nevertheless, the present CGCD analysis clearly shows that preheating has a pronounced impact on the effective glow curve composition of $NaCa_4(BO_3)_3$:Tb, highlighting the important role of shallow, metastable traps in governing the complexity of the TL response prior to thermal treatment. In this context, it is important to note that the activation energies obtained from heating-rate-based methods and those derived from CGCD analysis are not expected to coincide quantitatively, as they probe different aspects of the TL process.

The Hoogenstraaten VHR and BBP methods yield effective activation energies around ∼1.8–2.3 eV for the main TL peak, whereas the dominant CGCD components in the 260–280 °C region are centered around ∼1.58–1.63 eV. This discrepancy indicates that the apparent single dosimetric peak is not strictly isolated but remains composite, consisting of unresolved overlapping components and a distributed trap spectrum.

In such multi-trap systems, the fundamental assumption of an isolated peak inherent to VHR and BBP methods is not fully satisfied. As a result, heating-rate-based methods are biased toward the deepest and most slowly emptying sub-component that controls the Tm–β shift, whereas CGCD reflects the intensity-weighted contributions of multiple overlapping components forming the peak maximum. Therefore, the higher activation energy obtained from VHR/BBP should be interpreted as an effective "last-trap" parameter governing the peak shift, rather than the activation energy of a single discrete trapping level. This interpretation is fully consistent with the T_M–T_{stop} and Initial Rise results, which indicate a quasi-continuous distribution of trap depths extending up to ∼1.7 eV. In contrast, CGCD resolves the glow curve into multiple phenomenological components representing thermally accessible trapping levels contributing to the observed emission, particularly after preheating. Consequently, the higher effective *E* values obtained from VHR/BBP and the lower E range extracted from CGCD should be regarded as complementary rather than contradictory descriptions of a complex multi-trap system.

The kinetic parameters reported in Tables 2 and 3 correspond to point estimates obtained from nonlinear least-squares fitting. Formal uncertainties are not included because the large number of overlapping components and strong parameter correlations lead to an ill-conditioned covariance matrix, making individual parameter uncertainties difficult to interpret physically. The reported activation energies should therefore be regarded as effective values, consistent with the energy ranges independently obtained from T_M–T_{stop} and Initial Rise analyses.

5. Time-dependent TL enhancement and delayed fading: evidence for Trap–Center competition in $NaCa_4(BO_3)_3$:Tb

$NaCa_4(BO_3)_3$:Tb exhibits a highly unconventional post-irradiation TL evolution that cannot be described by simple, monotonically decaying first-order fading models. Instead, the material shows a pronounced time-dependent enhancement of the TL signal at a fixed glow-peak temperature, followed by delayed fading at extended storage times. Such non-monotonic behavior suggests a complex interplay of traps and recombination centers, rather than simple first-order emptying of a single, isolated trap (Chen and Hag-Yahya, 1997; Lawless et al., 2022; Chen, 2019; Benavente et al., 2024).

Fig. 10a presents the TL glow curves recorded after different waiting times following irradiation, measured after a preheating (preconditioning) treatment at 225 °C for 7 s. For all storage times, a single dominant glow peak centered at approximately 270 °C is observed, and both the peak position and overall glow-curve shape remain essentially unchanged, while only the peak intensity varies. The invariance of the glow-peak temperature strongly indicates that the dominant trapping level responsible for TL emission is thermally stable and that no significant modification of its trap depth or kinetic order occurs during storage. Such decoupling between peak temperature and effective lifetime is reminiscent of classical anomalous-fading behavior in feldspars and related materials, where high-temperature TL peaks can fade much faster than expected from their activation energies due to competition and complex center interactions (Lawless et al., 2022; Wintle, 1977). In this sense, $NaCa_4(BO_3)_3$:Tb shows similarities to anomalous-fading systems, while exhibiting a particularly pronounced and well-resolved intensity-enhancement (anti-fading) phase compared with most conventional dosimetric phosphors. To quantify this effect, the integrated TL glow-curve area as a function of storage time is shown in Fig. 10b. The TL response initially exhibits a low and nearly constant value immediately after irradiation, then undergoes a substantial increase exceeding an order of magnitude, before decreasing again at long storage times. This clearly reveals a non-monotonic temporal evolution with three distinct stages:

(i) an initial regime with weak TL, where the main trap is only partially filled and/or inefficiently coupled to radiative recombination centers; (ii) an intermediate regime where TL intensity grows strongly with storage time (anti-fading), consistent with time-dependent feeding of the main trap from auxiliary defect states (shallower traps, metastable centers, or deep competitors) through thermally assisted transfer, tunneling-mediated processes, or their combination; (iii) a late-time regime where both the main and auxiliary reservoirs become progressively depleted, leading to conventional fading dominated by non-radiative loss or slow thermal detrapping.

The initial suppressed TL signal suggests that a considerable fraction of charge carriers is trapped in TL-inactive or weakly radiative metastable states immediately after irradiation. With increasing storage time at room temperature, a gradual redistribution of charge carriers occurs, leading to an increased population of TL-active traps and/or more efficient recombination pathways involving Tb^{3+} luminescence centers. Because the enhancement appears without intentional thermal stimulation and proceeds over extended timescales at (or near) ambient temperature, a purely thermally activated activated first-order detrapping process alone is unlikely to account for the observed timescales and non-monotonic intensity evolution. It should be emphasized that, even after preheating at 225 °C for 7 s, the T_M–T_{stop} and CGCD analyses indicate the presence of deeper and metastable traps in the ~1.4–1.7 eV range that are not fully emptied by this short thermal treatment. Therefore, the time-dependent increase of the ~270 °C peak is attributed to charge transfer from these residual metastable/deeper auxiliary traps and/or competing centers, rather than from the very shallow traps removed during the preheating stage.

Within this context, a tunneling-assisted charge-transfer scenario represents one physically consistent framework capable of explaining the observed behavior. In this picture, charge carriers can migrate between spatially correlated traps or from metastable traps toward radiatively efficient recombination centers via quantum tunneling, even at low temperatures. Quantum-mechanical tunneling between localized states is well established as an important mechanism in the time-dependent TL and OSL behavior of feldspars and related minerals, where it can generate non-monotonic or intensity-enhancing effects without shifting glow-peak positions (Pagonis et al., 2020; Chen and Pagonis, 2020). In particular, Pagonis et al. (2020) demonstrated that in feldspars used for thermochronometry, quantum tunnelling between clustered traps and recombination centers controls the effective lifetime and leads to strong decoupling between apparent trap depth and fading rate, a situation closely analogous to the fixed-temperature, time-dependent intensity evolution observed here in $NaCa_4(BO_3)_3$:Tb (Pagonis et al., 2020). Similarly, competition-based models and OTOR-type approaches developed by Pagonis, Chen and co-workers predict non-exponential, sometimes non-monotonic luminescence behaviour controlled by trap–center topology rather than a single activation energy (Pagonis and Kitis, 2012). In such models, the apparent trap parameters inferred from conventional analysis can be misleading, because the effective lifetime is controlled by tunnelling distances and the spatial configuration of traps and recombination centers rather than by a single activation energy. The phenomenology observed in $NaCa_4(BO_3)_3$:Tb—intensity enhancement at an essentially fixed peak temperature followed by delayed fading—is therefore qualitatively compatible with a tunnelling-assisted redistribution of carriers among a network of traps and centers.

However, tunnelling should not be regarded as the only possible

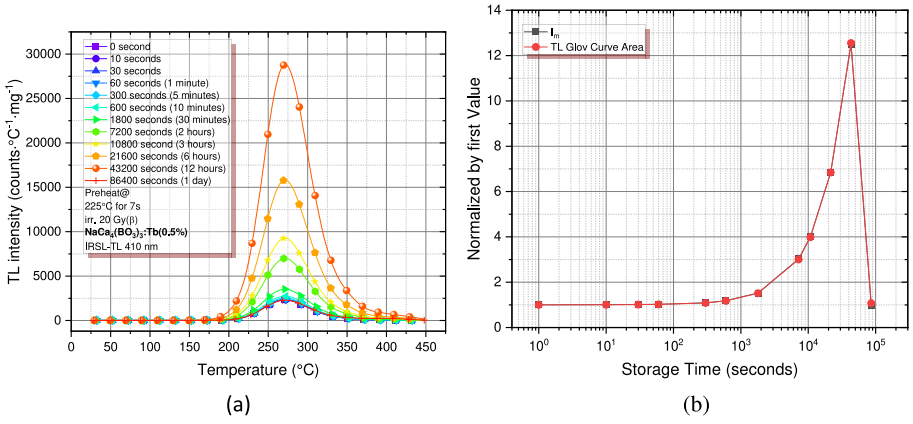

Fig. 10. (a) TL glow curves of preconditioned $NaCa_4(BO_3)_3$:Tb (0.5%) recorded at different storage times after irradiation (preheat at 225 °C for 7 s). (b) Storage-time dependence of the integrated TL glow curve area, showing pronounced time-dependent TL enhancement (anti-fading) followed by delayed fading at longer times.

mechanism. Alternative or concurrent processes—including defect relaxation, local structural rearrangements, delayed activation or stabilization of Tb^{3+}-related luminescence centers, and competitive trapping–retrapping dynamics—may also contribute to the observed enhancement. Similar behaviour has been discussed in models that reinterpret anomalous fading as "normal fading in disguise," caused by competition with non-radiative centers, which can narrow TL peaks and yield artificially large apparent activation energies and lifetimes (Chen and Pagonis, 2020). Multi-center and deep-trap competition models show that charge migration between localized levels, or between main and deep traps, can strongly distort the expected time evolution of TL and OSL signals without necessarily shifting glow-peak positions Kortov et al. (2006). Moreover, temperature-triggered luminescence enhancement due to the release of defect-trapped electrons and accelerated energy transfer has been reported in Tb,Eu-doped SrAlOCl phosphors, demonstrating that defect-mediated feeding of luminescent centers can produce pronounced intensity maxima while leaving the spectral and kinetic signatures largely unchanged (Kang et al., 2018). These studies reinforce the view that complex defect networks and competitive recombination pathways can readily produce anti-fading and anomalous fading effects similar to those observed in $NaCa_4(BO_3)_3$:Tb.

Viewed against the broader literature, the three-stage, time-dependent TL enhancement and delayed fading observed in $NaCa_4(BO_3)_3$:Tb can be interpreted as a macroscopic signature of carrier exchange between a thermally stable main TL trap and a network of auxiliary traps and recombination centers. This behaviour is governed by trap–center competition and non-radiative pathways, with tunnelling-mediated localized transitions representing a possible contributing mechanism, and is not readily explained by simple first-order fading of an isolated trap.

The present study focuses on a single irradiation dose (20 Gy) and preheated samples; temporal evolution without preheating and the explicit dose dependence of the anti-fading effect were not investigated here and remain subjects for future work. For this reason, Fig. 10b is interpreted qualitatively as evidence of non-monotonic TL evolution in a competitive multi-trap system, without attempting a detailed quantitative fit to a specific kinetic model.

The CGCD analysis of the pre-preheated sample requires multiple overlapping components (13 peaks) with activation energies distributed between ~1.0 and ~1.8 eV, confirming a complex multi-trap structure rather than a single discrete trapping level. The anomalous anti-fading behaviour is therefore interpreted in terms of charge redistribution and competition within this multi-trap network. While the coexistence of multiple trapping components and two crystalline phases may in principle allow interphase interactions, the present interpretation remains phenomenological. A rigorous microscopic attribution of individual TL components to specific defects or phases would require phase-pure reference samples and advanced spectroscopic techniques (e.g., ESR), which are beyond the scope of this first systematic TL and kinetic investigation of $NaCa_4(BO_3)_3$:Tb^3.

6. Conclusions

The TL behavior of Tb^{3+}-doped $NaCa_4(BO_3)_3$ has been systematically examined in terms of trap structure, preheating effects and time-dependent signal evolution. T_m–T_{stop} measurements combined with Initial Rise analysis, heating-rate-based methods and computerized glow-curve deconvolution consistently indicate that the material does not behave as a simple single-trap system, but instead exhibits a quasi-continuous distribution of trapping levels extending from shallow (~1.0 eV) to deeper states above ~1.6–1.7 eV, coupled to a dominant recombination center. This multi-trap architecture leads to a complex, initially multi-peak glow curve that can be effectively simplified by an appropriate thermal protocol.

A controlled preheating step at 225 °C for 7 s acts as a thermal cleaning stage that strongly reduces the contribution of low- and intermediate-temperature peaks near 80 °C and 190 °C, while largely preserving a deeper, high-temperature peak around 260–270 °C. T_M–T_{stop}/Initial Rise and CGCD analyses before and after preheating indicate that this procedure predominantly depletes the most unstable shallow traps with activation energies below ~1.1 eV, while deeper and metastable trapping levels in the ~1.5–1.8 eV range are only partially affected. These results suggest that preheating is essential for stabilizing the main dosimetric peak and reducing glow-curve complexity in $NaCa_4(BO_3)_3$:Tb.

Time-resolved storage experiments reveal a pronounced non-monotonic TL evolution of the isolated high-temperature peak: the peak intensity initially increases by more than an order of magnitude with storage time at room temperature and subsequently decreases at longer times, while the peak temperature and overall shape remain essentially unchanged. This behavior is attributed to charge redistribution and trap competition within a multi-trap network involving shallow, metastable and deeper states, rather than simple first-order emptying of a single trap, although a unique microscopic mechanism cannot be established from the present data. The observed non-monotonic TL evolution is attributed to charge redistribution within a competitive multi-trap system, while a detailed microscopic mechanism remains beyond the scope of the present work.

From a dosimetric perspective, the preheated material exhibits a single, high-temperature peak with a linear dose response from ~1.4 at least 350 Gy, stable peak position, and good readout reproducibility over repeated cycles. These characteristics indicate that Tb^{3+}-doped $NaCa_4(BO_3)_3$ is a potential candidate for high-dose β-radiation dosimetry within the conditions investigated in this study, provided that practical protocols explicitly include a standardized preheating step and controlled storage times to account for the observed time-dependent enhancement and delayed fading. A direct comparison with established TL dosimeters such as LiF:Mg,Ti (TLD-100), $CaSO_4$:Dy, or $Li_2B_4O_7$:Cu was not performed in this study and remains an important subject for future work.

The CGCD analysis of the pre-preheated sample requires multiple overlapping components with activation energies distributed between ~1.0 and ~1.8 eV, confirming a complex multi-trap structure rather than a single discrete trapping level. The anomalous anti-fading behaviour is interpreted in terms of charge redistribution and competition within this multi-trap network. While the coexistence of multiple trapping components and two crystalline phases may in principle allow interphase interactions, the present interpretation remains phenomenological. A rigorous microscopic attribution of individual TL components to specific defects or phases would require phase-pure reference samples and advanced spectroscopic techniques (e.g., ESR), which are beyond the scope of this first systematic TL and kinetic investigation of $NaCa_4(BO_3)_3$:Tb^{3+}. Further optimization of synthesis conditions to achieve phase-pure samples will be considered in future studies.

CRediT authorship contribution statement

Kenan Bulcar: Formal analysis, Investigation, Methodology. **E. Aymila Cin:** Formal analysis, Investigation, Methodology. **Abeer S. Altowyan:** Formal analysis, Funding acquisition, Investigation, Methodology, Writing – original draft. **M.B. Coban:** Formal analysis, Investigation, Methodology. **U.H. Kaynar:** Formal analysis, Investigation, Methodology. **H. Orucu:** Investigation, Methodology, Software. **Jabir Hakami:** Conceptualization, Investigation, Methodology. **Mustafa Topaksu:** Conceptualization, Investigation, Methodology. **M. Ayvacikli:** Conceptualization, Investigation, Methodology. **N. Can:** Conceptualization, Writing – original draft, Writing – review & editing.

Declaration of competing interest

The authors declare that they have no known competing financial interests or personal relationships that could have appeared to influence

the work reported in this paper.

Acknowledgement

This study was supported by the Princess Nourah bint Abdulrahman University Researchers Supporting Project number (PNURSP2026R16), Princess Nourah bint Abdulrahman University, Riyadh, Saudi Arabia. This study is supported by Scientific Research Projects Coordination Unit of Ege University (Project Number: 32607) and by the Turkish Scientific Research Council with the project numbered "223M036" within the scope of the"TUBITAK-1001″ project.

Data availability

Data will be made available on request.

References

Ahadova, A., 2024. Temperature effect on thermoluminescence kinetic parameters of nano-alumina. Adv. Phys. Res. 6, 239–246. https://doi.org/10.62476/apr63239.

Alajlani, Y., Oglakci, M., Kaynar, U.H., Ayvacikli, M., Portakal-Uçar, Z.G., Topaksu, M., Can, N., 2021. Thermoluminescence study and evaluation of trapping parameters of samarium doped barium silicate phosphor. J. Asian Ceram. Soc. 9, 291–303. https://doi.org/10.1080/21870764.2020.1864898.

Altowyan, A.S., Kaynar, Ü.H., Bulcar, K., Oglakci, M., Portakal-Uçar, Z.G., Hakami, J., Topaksu, M., Can, N., 2023. Unusual heating rates, dose responses and kinetic parameters detected on thermoluminescence from $YAl_3(BO_3)_4:Sm^{3+}$ phosphors. Ceram. Int. 49, 33291–33304. https://doi.org/10.1016/j.ceramint.2023.08.038.

Altowyan, A.S., Sonsuz, M., Kaynar, U.H., Hakami, J., Portakal-Uçar, Z.G., Ayvacikli, M., Topaksu, M., Can, N., 2024. Synthesis and thermoluminescence behavior of novel Sm^{3+} doped $YCa_4O(BO_3)_3$ under beta irradiation. Ceram. Int. 50, 19681–19691. https://doi.org/10.1016/j.ceramint.2024.03.089.

Anishia, S.R., Jose, M.T., Annalakshmi, O., Ponnusamy, V., Ramasamy, V., 2010. Dosimetric properties of rare earth doped $LiCaBO_3$ thermoluminescence phosphors. J. Lumin. 130, 1834–1840. https://doi.org/10.1016/j.jlumin.2010.04.019.

Anishia, S.R., Jose, M.T., Annalakshmi, O., Ramasamy, V., 2011. Thermoluminescence properties of rare earth doped lithium magnesium borate phosphors. J. Lumin. 131, 2492–2498. https://doi.org/10.1016/j.jlumin.2011.06.019.

Başaran, B.Y., Kafadar, V.E., Emen, F.M., Öztürk, E., Karaçolak, A.İ., 2025. Photoluminescence and thermoluminescence studies of beta-irradiated $Ba_3CdSi_2O_8:Tb^{3+}$ phosphor for LED and dosimetry applications. Luminescence 40. https://doi.org/10.1002/bio.70171.

Benavente, J.F., Arquero, O., Berenguer-Antequera, J., 2024. Effects of trapped charge transitions between localized levels on the optical properties of thermoluminescent materials: a study of fading and thermal quenching. Opt. Mater. 156, 116006. https://doi.org/10.1016/j.optmat.2024.116006.

Benavente, J.F., Gómez-Ros, J.M., Correcher, V., 2020. Characterization of the thermoluminescence glow curve of $Li_2B_4O_7$:Cu,Ag. Radiat. Meas. 137, 106427. https://doi.org/10.1016/j.radmeas.2020.106427.

Bilski, P., 2002. Lithium fluoride: from LiF:Mg,Ti to LiF:Mg,Cu,P. Radiat. Protect. Dosim. 100, 199–205. https://doi.org/10.1093/oxfordjournals.rpd.a005847.

Bohun, A., 1954. Thermoemission und photoemission von natriumchlorid, Czechoslov. J. Phys. 4, 91–93.

Booth, A.H., 1954. Calculation of electron trap depth from thermoluminescence maxima. Can. J. Chem. 32, 214–215.

Can, N., Townsend, P.D., Wang, Y., 2025. Analytical benefits from logarithmic displays of luminescence sensitivity. Vacuum 238, 114273. https://doi.org/10.1016/j.vacuum.2025.114273.

Chen, R., 2019. Recent advances in the theory of thermoluminescence and optically stimulated luminescence; delocalized transitions. In: Adv. Phys. Appl. Opt. Therm. Stimul. Lumin., World Scientific (Europe), pp. 1–36. https://doi.org/10.1142/9781786345790_0001.

Chen, R., Hag-Yahya, A., 1997. A new possible interpretation of the anomalous fading in thermoluminescent materials as normal fading in disguise. Radiat. Meas. 27, 205–210. https://doi.org/10.1016/S1350-4487(96)00147-3.

Chen, R., McKeever, S.W.S., 2011. Theory of Thermoluminescence and Related Phenomena. World Scientific, Singapore.

Chen, R., Pagonis, V., 2020. A Monte-Carlo study of the fading of TL and OSL signals in the presence of deep-level competitors. Radiat. Meas. 132, 106257. https://doi.org/10.1016/j.radmeas.2020.106257.

Coban, M.B., Kaynar, U.H., Altowyan, A.S., Hakami, J., Aydin, H., Canimoglu, A., Can, N., 2025. Judd–Ofelt analysis and negative thermal quenching behavior of Tb^{3+}-activated $Ca_3La_3(BO_3)_5$ phosphors co-doped with alkali ions for high-temperature photonic applications. Sensors Actuators A Phys 395, 117109. https://doi.org/10.1016/j.sna.2025.117109.

Del Sol Fernández, S., García-Salcedo, R., Mendoza, J.G., Sánchez-Guzmán, D., Rodríguez, G.R., Gaona, E., Montalvo, T.R., 2016. Thermoluminescent characteristics of LiF:Mg, Cu, P and $CaSO_4$:Dy for low dose measurement. Appl. Radiat. Isot. 111, 50–55. https://doi.org/10.1016/j.apradiso.2016.02.011.

Delice, S., 2018. Temperature lag effect on TL glow peaks: corrections on kinetic parameters. J. Lumin. 204, 81–88. https://doi.org/10.1016/j.jlumin.2018.07.044.

Etefa, H.F., Mbuyise, X.G., Geldasa, F.T., Mola, G.T., Chithambo, M.L., Dejene, F.B., 2025. The influence of energy levels and defects on the thermoluminescence of LiF:SiO_5 phosphors doped with Ce^{3+}. Int. J. Mol. Sci. 26, 3183. https://doi.org/10.3390/ijms26073183.

Gavhane, K.H., Bhadane, M.S., Bhoir, A.S., Kulkarni, P.P., Patil, B.J., Bhoraskar, V.N., Dhole, S.D., Dahiwale, S.S., 2020. Tm-Tstop analysis and dosimetric properties of Ce doped BaB_4O_7 phosphor. J. Alloys Compd. 817, 152805. https://doi.org/10.1016/j.jallcom.2019.152805.

Gieszczyk, W., Marczewska, B., Kłosowski, M., Mrozik, A., Bilski, P., Sas-Bieniarz, A., Goj, P., Stoch, P., 2019. Thermoluminescence enhancement of $LiMgPO_4$ crystal host by Tb^{3+} and Tm^{3+} trivalent rare-earth ions Co-doping. Materials 12, 2861. https://doi.org/10.3390/ma12182861.

Guo, J., Jian, C., Zeng, C., Xiong, Z., Wang, L., Zhou, D., 2023. Dosimetric and spectroscopic study of $LiMgPO_4$ doped with Tm^{3+} and Er^{3+}. RSC Adv. 13, 4949–4957. https://doi.org/10.1039/D2RA07109F.

W. Hoogenstraaten, Electron traps in zinc-sulphide phosphors, Philips Res. Rep. 13 (n.d.) 515–693.

Jakathamani, S., Annalakshmi, O., Jose, M.T., 2018. Thermoluminescent properties of rare earth doped lithium strontium borate phosphors. https://doi.org/10.1063/1.5031742.

Jakathamani, S., Annalakshmi, O., Jose, M.T., Venkatraman, B., 2021. Thermoluminescence dosimetric characteristics of terbium doped barium metaborate phosphors. Radiat. Phys. Chem. 187, 109544. https://doi.org/10.1016/j.radphyschem.2021.109544.

Jena, M., Sen, D., Zulfequar, M., Asokan, K., Pandey, A., 2023. Study of the thermoluminescence properties of γ and UV-C irradiated Li_3PO_4: dy synthesized by solid state diffusion method. J. Alloys Compd. 955, 170077. https://doi.org/10.1016/j.jallcom.2023.170077.

Joseph, T.A., Chopra, V., Dhoble, S.J., 2023. Thermoluminescence studies of zinc borate (ZnB_2O_4) phosphor doped with rare earths for dosimetric aspects. Luminescence 38, 1597–1606. https://doi.org/10.1002/bio.4542.

Kadari, A., Faria, L.O., Kadri, D., Khaidukov, N.M., 2013. Modeling of the TL response of K_2YF_5 for different concentrations of Tb^{3+} ions. J. Lumin. 143, 574–578. https://doi.org/10.1016/j.jlumin.2013.06.018.

Kalita, J.M., Chithambo, M.L., 2017. Thermoluminescence of α-Al_2O_3:C,Mg: kinetic analysis of the main glow peak. J. Lumin. 182, 177–182. https://doi.org/10.1016/j.jlumin.2016.10.031.

Kameshwaran, R., Annalakshmi, O., K, A., Bhargav, P.B., 2023. Novel green emitting Tb^{3+} doped $KCaF_3$ phosphor for WLEDs and TLD applications. Ceram. Int. 49, 8005–8014. https://doi.org/10.1016/j.ceramint.2022.10.316.

Kang, F., Sun, G., Wang, A., Xiao, X., Li, Y.Y., Lu, J., Huang, B., 2018. Multicolor tuning and temperature-triggered anomalous Eu^{3+} -Related photoemission enhancement via interplay of accelerated energy transfer and release of defect-trapped electrons in the Tb^{3+} ,Eu^{3+} -Doped strontium–aluminum chlorites. ACS Appl. Mater. Interfaces 10, 36157–36170. https://doi.org/10.1021/acsami.8b13728.

Kaynar, S.C., Altowyan, A.S., Aydin, H., Kaynar, U.H., Coban, M.B., Hakami, J., Can, N., 2025. Judd–Ofelt analysis and photoluminescence behavior of Tb^{3+}-activated $K_7SrY_2(B_5O_{10})_3$ phosphors modified with alkali co-dopants for solid-state lighting applications. Spectrochim. Acta Part A Mol. Biomol. Spectrosc. 341, 126435. https://doi.org/10.1016/j.saa.2025.126435.

Keskin, İ.Ç., İlhan, M., 2023. Thermoluminescence kinetic parameters and radioluminescence of RE^{3+} (RE = Pr, Sm, Tb, Ho, Er)-Doped barium tantalate phosphors. J. Electron. Mater. 52, 5614–5630. https://doi.org/10.1007/s11664-023-10501-y.

Khan, Z.S., Ingale, N.B., Omanwar, S.K., 2016. Synthesis and thermoluminescence properties of rare earth-doped $NaMgBO_3$ phosphor. Environ. Sci. Pollut. Res. 23, 9295–9302. https://doi.org/10.1007/s11356-015-4993-6.

Kiran, R., Kamath, N., Sayyed, M.I., Almuqrin, A.H., Kamath, S.D., 2025. A review of recent developments in rare earth-doped nanophosphors for emerging technological applications. RSC Adv. 15, 20040–20060. https://doi.org/10.1039/D5RA03126E.

Kitis, G., Gomez-Ros, J.M., Tuyn, J.W.N., 1998. Thermoluminescence glow-curve deconvolution functions for first, second and general orders of kinetics. J. Phys. D Appl. Phys. 31, 2636–2641. https://doi.org/10.1088/0022-3727/31/19/037.

Kitis, G., Tuyn, J.W.N., 1998. A simple method to correct for the temperature lag in TL glow-curve measurements. J. Phys. D Appl. Phys. 31, 2065–2073. https://doi.org/10.1088/0022-3727/31/16/017.

Kortov, V.S., Milman, I.I., Moiseykin, E.V., Nikiforov, S.V., Ovchinnikov, M.M., 2006. Deep-trap competition model for TL in α-Al_2O_3:C heating stage. Radiat. Protect. Dosim. 119, 41–44. https://doi.org/10.1093/rpd/nci544.

Kumar, P., Singh, D., Gupta, I., Singh, S., Nehra, S., Kumar, R., 2023. Combustion derived single phase $Y_4Al_2O_9:Tb^{3+}$ nanophosphor: crystal chemistry and optical analysis for solid state lighting applications. RSC Adv. 13, 7752–7765. https://doi.org/10.1039/D3RA00735A.

Lawless, J.L., Chen, R., Pagonis, V., 2022. A model explaining the anomalous fading effect in thermoluminescence (Tl). SSRN Electron. J. https://doi.org/10.2139/ssrn.4158321.

Li, R., Li, H., Chang, C., Sun, Z., 2022. Enhanced afterglow behavior of a new Eu^{2+}:$NaBa_4(BO_3)_3$ yellow phosphor co-doped with different cations Dy^{3+}, $Ho^{3+}$and Nd^{3+}. Ceram. Int. 48, 8914–8920. https://doi.org/10.1016/j.ceramint.2021.12.267.

Liu, L., Zhang, Y., Hao, J., Li, C., Tang, Q., Zhang, C., Su, Q., 2005. Thermoluminescence characteristics of terbium-doped $Ba_2Ca(BO_3)_2$ phosphor. Phys. Status Solidi 202, 2800–2806. https://doi.org/10.1002/pssa.200521199.

Liuzzi, R., Piccolo, C., D'Avino, V., Clemente, S., Oliviero, C., Cella, L., Pugliese, M., 2020. Dose–response of TLD-100 in the dose range useful for hypofractionated radiotherapy. Dose Response 18. https://doi.org/10.1177/1559325819894081.

Madkhali, O., Bulcar, K., Barad, A., Zelai, T., Souadi, G., Alathlawi, H.J., Kaynar, U.H., Topaksu, M., Can, N., 2025. Thermoluminescence behaviour and kinetic analysis of a novel Tb^{3+}-Doped $LaCa_4O(BO_3)_3$ phosphor: impacts of heating rates and dose. Mater. Sci. Semicond. Process. 187, 109132. https://doi.org/10.1016/j.mssp.2024.109132.

Mammadov, S., Gurbanov, M., Ahadov, A., 2024. Exploring the thermoluminescent characteristics of nano α-Al_2O_3: influence of heating rate on glow peaks and activation energy. Eur. J. Chem. 15, 149–154. https://doi.org/10.5155/eurjchem.15.2.149-154.2552.

McKeever, S.W.S., 1980. On the analysis of complex thermoluminescence. Glow-curves: resolution into individual peaks. Phys. Status Solidi 62, 331–340. https://doi.org/10.1002/pssa.2210620139.

McKeever, S.W.S., 1985. Thermoluminescence of Solids. Cambridge University Press, Cambridge.

Ngoc, T., Ca, N.X., Ha, N.V., Thuy, T.T.C., Huong, N.T., Thanh, L.D., Van Nghia, N., Van Do, P., 2025. Thermoluminescence properties of the $Li_2B_4O_7$:Dy^{3+},Ce^{3+} glasses and their application potential in the dosimetry field. Opt. Mater. 158, 116443. https://doi.org/10.1016/j.optmat.2024.116443.

Niyonzima, P., Oehler, S., King, G.E., Schmidt, C., 2024. Investigating thermoluminescence signal saturation in quartz and feldspar using emission spectrometry. Radiat. Meas. 177, 107262. https://doi.org/10.1016/j.radmeas.2024.107262.

Oglakci, M., Akça-Özalp, S., Portakal-Uçar, Z.G., Correcher, V., Benavente, J.F., Sonsuz, M., Can, N., Halefoglu, Y.Z., Topaksu, M., 2025. Thermoluminescence study of Nd^{3+} doped lanthanum tri-borate phosphor. J. Alloys Compd. 1013, 178570. https://doi.org/10.1016/j.jallcom.2025.178570.

Oglakci, M., Portakal-Uçar, Z.G., Akça-Özalp, S., Correcher, V., Benavente, J.F., Sonsuz, M., Can, N., Halefoglu, Y.Z., Topaksu, M., 2023. Thermoluminescence behavior of Ce^{3+} doped lanthanum tri-borate phosphor for dosimetry applications. Ceram. Int. 49, 36092–36102. https://doi.org/10.1016/j.ceramint.2023.08.288.

Ono, H., Fujimoto, Y., Yahaba, T., Yanagida, T., Koshimizu, M., Asai, K., 2019. Thermoluminescence properties of Tb^{3+}-doped CaO–Al_2O_3–B_2O_3-based glasses. Opt. Mater. 87, 24–28. https://doi.org/10.1016/j.optmat.2018.07.004.

Oza, A., Ojha, V., Dhale, S., Dhoble, S., 2022. Photoluminescence and thermoluminescence in Dy^{3+}-, Ce^{3+} -, and Tb^{3+} -activated MgB_4O_7 phosphor for dosimetry application. Luminescence 37, 1563–1574. https://doi.org/10.1002/bio.4332.

Pagonis, V., Kitis, G., Furetta, C., 2006. Numerical and Practical Exercises in Thermoluminescence. Springer New York, New York, NY. https://doi.org/10.1007/0-387-30090-2.

Pagonis, V., Kitis, G., Polymeris, G.S., 2020. Quantum tunneling processes in feldspars: using thermoluminescence signals in thermochronometry. Radiat. Meas. 134, 106325. https://doi.org/10.1016/j.radmeas.2020.106325.

Pagonis, V., Kitis, G., 2012. Prevalence of first-order kinetics in thermoluminescence materials: an explanation based on multiple competition processes. Phys. Status Solidi 249, 1590–1601. https://doi.org/10.1002/pssb.201248082.

Parfianovitch, I.A., 1954. The determination of the depth of electron traps in crystal phosphors. J. Exp. Theor. Phys. 26, 696.

Pathan, S., Dubey, P., Tadge, P., Ray, S., 2022. A comprehensive review on rare-earth based thermoluminescence phosphors for radiation dosimetry. ECS Trans. 107, 20073–20084. https://doi.org/10.1149/10701.20073ecst.

Peng, J., Dong, Z., Han, F., 2016. tgcd: an R package for analyzing thermoluminescence glow curves. SoftwareX 5, 112–120. https://doi.org/10.1016/j.softx.2016.06.001.

Portakal-Uçar, Z.G., Oglakci, M., Correcher, V., Sonsuz, M., Can, N., Halefoglu, Y.Z., Topaksu, M., 2023. A thermoluminescence study of Tb^{3+} doped LaB_3O_6: dosimetric characteristics and kinetic parameters. J. Lumin. 253, 119493. https://doi.org/10.1016/j.jlumin.2022.119493.

Reddy, S.S., Nagabhushana, K.R., Tatumi, S.H., Thejavathi, N.R., 2025. Investigating the optical and thermoluminescence properties of γ-irradiated Al_2O_3:Tb^{3+} phosphors for dosimetric applications. J. Lumin. 280, 121067. https://doi.org/10.1016/j.jlumin.2025.121067.

Richter, D., Richter, A., Dornich, K., 2015. Lexsyg smart — a luminescence detection system for dosimetry, material research and dating application. Geochronometria 42, 202–209. https://doi.org/10.1515/geochr-2015-0022.

Romero, C., Rivera, T., Calderón Arenas, J.A., Sadek, A., 2026. TLDecPy: an open python framework for robust thermoluminescence glow-curve deconvolution and metrological uncertainty quantification. https://doi.org/10.2139/ssrn.6342751.

Sadek, A.M., Eissa, H.M., Basha, A.M., Kitis, G., 2015. Properties of the thermoluminescence glow peaks simulated by the interactive multiple-trap system (IMTS) model. Phys. Status Solidi 252, 721–729. https://doi.org/10.1002/pssb.201451406.

Salas-Juárez, C.J., Ugalde-Valdés, M.A., Guzmán-Mendoza, J., Nolasco-Altamirano, D., Martínez-Gil, M., Gómez-Dominguez, C.E., Guarin, C.A., Melendrez, R., Rivera-Montalvo, T., 2023. Persistent luminescence of commercial TLD-100 dosimeter: using shallow traps for radiation dosimetry. Radiat. Meas. 167, 106997. https://doi.org/10.1016/j.radmeas.2023.106997.

Saran, M., Sahare, P.D., Ali, N., 2025. Thermoluminescence of $NaLi_2PO_4$:Ce^{3+} TLD phosphor for estimation of high doses of high-energy radiation: effects of particle size. J. Radioanal. Nucl. Chem. 334, 6529–6544. https://doi.org/10.1007/s10967-024-09864-1.

Satkar, R.C., Kadam, A.R., Ovhal, D.A., Dhoble, S.J., 2021. Inorganic thermoluminescent phosphors in radiation dosimetry: an overview. J. Phys., Conf. Ser. 1913, 012023. https://doi.org/10.1088/1742-6596/1913/1/012023.

Shi, M., Zhu, C., Wei, M., He, Z., Lu, M., 2018a. Dy^{3+}-, Tb^{3+}-, and Eu^{3+}-activated $NaCa_4(BO_3)_3$ phosphors for lighting based on near ultraviolet light emitting diodes. Vacuum 149, 343–349. https://doi.org/10.1016/j.vacuum.2018.01.014.

Shi, M., Zhu, C., Zhang, M., Lu, M., Liu, J., 2018b. $NaCa_4(BO_3)_3$:Ce, Dy, Eu phosphors for light emitting diode applications. Polyhedron 140, 19–24. https://doi.org/10.1016/j.poly.2017.10.021.

Singh, S., Singh, D., 2021. Structural and optical properties of green emitting Y_2SiO_5:Tb^{3+} and Gd_2SiO_5:Tb^{3+} nanoparticles for modern lighting applications. Rare Met. 40, 3289–3298. https://doi.org/10.1007/s12598-020-01585-0.

Sonsuz, M., Topaksu, M., Hakami, J., Can, N., 2022. Synthesis and thermoluminescence study of Eu doped novel $LaBO_3$ phosphor: heating rate, dose response, trapping parameters. Radiat. Phys. Chem. 201, 110412. https://doi.org/10.1016/j.radphyschem.2022.110412.

Touliopoulos, A., Kitis, G., 2025. Simulation of peak properties in thermoluminescence dosimeters with the potential stimulation of all electron traps. Radiat. Phys. Chem. 228, 112395. https://doi.org/10.1016/j.radphyschem.2024.112395.

Townsend, P.D., 1994. Analysis of TL emission spectra. Radiat. Meas. 23, 341–348. https://doi.org/10.1016/1350-4487(94)90062-0.

Van der Heggen, D., Vandenberghe, D., Moayed, N.K., De Grave, J., Smet, P.F., Joos, J.J., 2020. The almost hidden role of deep traps when measuring afterglow and thermoluminescence of persistent phosphors. J. Lumin. 226, 117496. https://doi.org/10.1016/j.jlumin.2020.117496.

Wang, L., Huang, J., Chen, L., Xiong, Z., Guo, J., 2025. Photoluminescence and thermoluminescence properties of rare earth Tm^{3+}, Dy^{3+} co-doped Y_2MgTiO_6 double perovskite phosphors. J. Lumin. 280, 121114. https://doi.org/10.1016/j.jlumin.2025.121114.

Wintle, A.G., 1977. Detailed study of a thermoluminescent mineral exhibiting anomalous fading. J. Lumin. 15, 385–393. https://doi.org/10.1016/0022-2313(77)90037-0.

Xiang, Y., Li, H., Zhang, H., Yang, L., Liao, C., Yang, T., Li, J., Guo, Z., Zhu, J., 2024. Microwave-assisted fast synthesis and red-emitting properties of a borotellurate-based phosphor with excellent thermostability. J. Rare Earths 42, 1036–1045. https://doi.org/10.1016/j.jre.2023.03.012.

Yukihara, E.G., Bos, A.J.J., Bilski, P., McKeever, S.W.S., 2022. The quest for new thermoluminescence and optically stimulated luminescence materials: needs, strategies and pitfalls. Radiat. Meas. 158, 106846. https://doi.org/10.1016/j.radmeas.2022.106846.